Journal of Medicinal Chemistry

Article

Cite This: J. Med. Chem. 2018, 61, 4087−4102

pubs.acs.org/jmc

Discovery of Inhibitor of Wnt Production 2 (IWP-2) and Related Compounds As Selective ATP-Competitive Inhibitors of Casein Kinase 1 (CK1) δ/ε

Balbina García-Reyes,[†] Lydia Witt,[‡] Björn Jansen,[‡] Ebru Karasu,[†] Tanja Gehring,[†] Johann Leban,[§] Doris Henne-Bruns,[†] Christian Pichlo,[∥] Elena Brunstein,[∥] Ulrich Baumann,[∥] Fabian Wesseler,[⊥] Bernd Rathmer,[⊥] Dennis Schade,[⊥,#] Christian Peifer,*[,‡] and Uwe Knippschild*[,†]

[†]Department of General and Visceral Surgery, Ulm University Hospital, Albert-Einstein-Allee 23, D-89081 Ulm, Germany

[‡]Institute of Pharmacy, Christian-Albrechts-University of Kiel, Gutenbergstraße 76, D-24116 Kiel, Germany

[§]Oncotyrol GmbH, Karl-Kapferer-Straße 5, 6020 Innsbruck, Austria

[∥]Department for Chemistry, University of Cologne, Zülpicher Str. 47B, D-50674 Cologne, Germany

[⊥]Department of Chemistry and Chemical Biology, TU Dortmund University, Otto-Hahn-Str. 6, D-44227 Dortmund, Germany

[#]Institute of Pharmacy, Ernst-Moritz-Arndt-University of Greifswald, Felix-Hausdorff-Str. 1, D-17489 Greifswald, Germany

Supporting Information

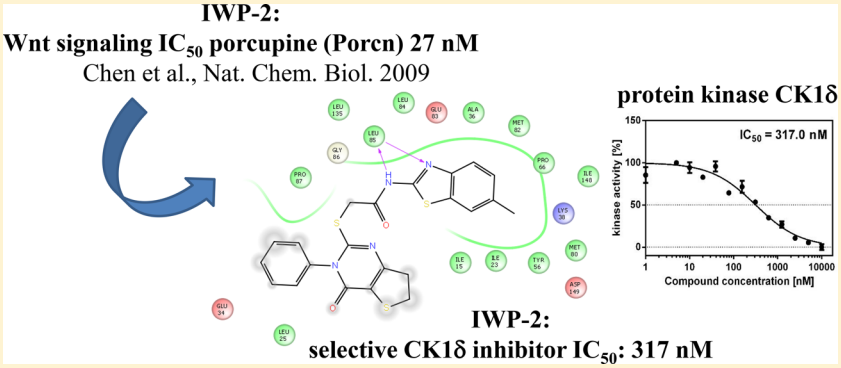

ABSTRACT: Inhibitors of Wnt production (**IWPs**) are known antagonists of the Wnt pathway, targeting the membrane-bound O-acyltransferase porcupine (Porcn) and thus preventing a crucial Wnt ligand palmitoylation. Since **IWPs** show structural similarities to benzimidazole-based CK1 inhibitors, we hypothesized that **IWPs** could also inhibit CK1 isoforms. Molecular modeling revealed a plausible binding mode of **IWP-2** in the ATP binding pocket of CK1δ which was confirmed by X-ray analysis. *In vitro* kinase assays demonstrated **IWPs** to be ATP-competitive inhibitors of ^{wt}CK1δ. **IWPs** also strongly inhibited the gatekeeper mutant ^{M82F}CK1δ. When profiled in a panel of 320 kinases, **IWP-2** specifically inhibited CK1δ. **IWP-2** and **IWP-4** also inhibited the viability of various cancer cell lines. By a medicinal chemistry approach, we developed improved **IWP**-derived CK1 inhibitors. Our results suggest that the effects of **IWPs** are not limited to Porcn, but also might influence CK1δ/ε-related pathways.

INTRODUCTION

Casein kinase 1 (CK1) is an ubiquitously expressed serine/threonine kinase family in mammals, known to phosphorylate a broad range of proteins.[1] Accordingly, CK1 isoforms play essential regulatory roles in diverse cellular processes including proliferation, DNA repair, apoptosis, cell differentiation, and circadian rhythm.[1−3] The CK1 family consists of different isoforms (α, γ1, γ2, γ3, δ, and ε) in humans, and their various alternative splice variants.[4] CK1 isoforms possess a highly conserved kinase domain but differ significantly in length and composition of their N- and C-terminal sequences.[5,6] Since deregulation of CK1 expression and activity contributes to the development of disorders such as cancer (CK1α/γ/δ/ε), neurodegenerative diseases (CK1δ), and inflammation (CK1α/δ/ε), there is an increased interest to develop CK1-specific inhibitors to be used as pharmacological tools and for new therapeutic approaches.[1]

One of the most prominent cellular processes involving regulation by CK1 is Wnt signaling, a rather complex group of signal transduction pathways controlling several processes including embryonic development and tissue homeostasis.[7,8] CK1 isoforms are involved in both negative and positive regulation of canonical as well as noncanonical Wnt path-

Received: January 19, 2018
Published: April 9, 2018

DOI: 10.1021/acs.jmedchem.8b00095
J. Med. Chem. 2018, 61, 4087−4102

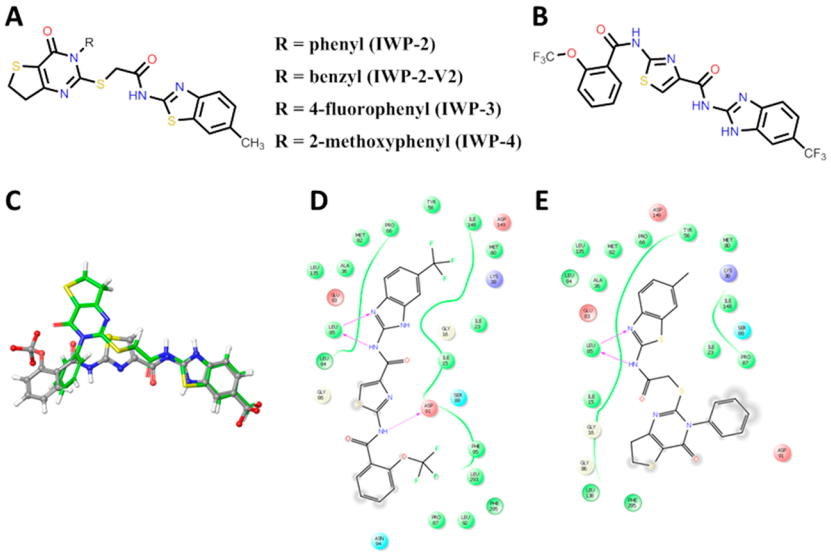

Figure 1. Structural similarities of IWP compounds and benzimidazole derivatives. (A) Chemical structures of **IWP** compounds. (B) Chemical structure of the benzimidazole CK1 inhibitor **Bischof-5**[20] (PDB 4TWC, rat CK1δ IC_{50} = 0.040 ± 0.01 μM, human CK1δ transcription variant 1 (TV1) IC_{50} 0.022 ± 0.02 μM, human CK1δ TV2 IC_{50} 0.042 ± 0.02 μM corresponding to compound **5**.[20] (C) Overlay of chemical structures of **IWP-2** (green) and benzimidazole CK1δ inhibitor **Bischof-5** (gray) to illustrate molecular similarities. (D) Binding mode of **Bischof-5** in CK1δ determined by X-ray analysis (PDB 4TWC, presented as 2D ligand interaction diagram LID). Key interactions are shown. (E) Modeled binding mode of **IWP-2** in CK1δ by docking the ligand into the active site of 4TWC (Glide, Schrödinger, presented as 2D LID).

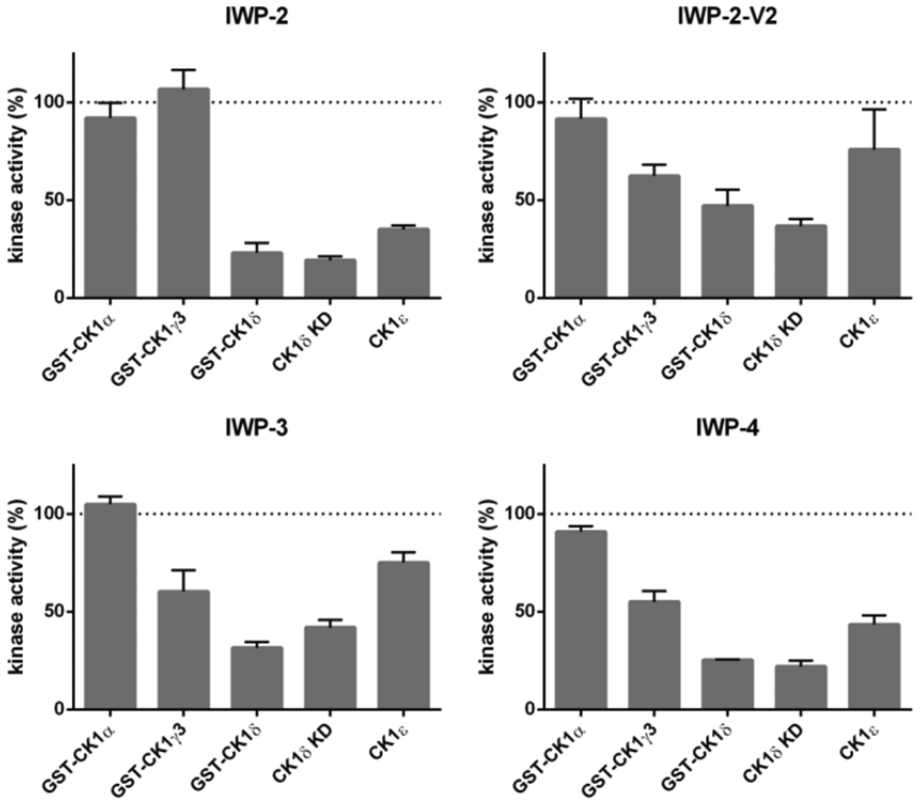

Figure 2. IWP derivatives specifically inhibit CK1δ isoform. *In vitro* kinase assays were performed in the presence or absence of **IWP-2**, **IWP-2-V2**, **IWP-3**, or **IWP-4** (10 μM) at a concentration of 10 μM ATP using either GST-CK1α (bovine), GST-CK1γ3 (human), GST-CK1δ (rat), CK1δKD (rat), or CK1ε (human) as enzymes and α-casein as substrate. Results are shown as normalized bar graphs using DMSO as a control for 100% kinase activity (dotted line).

ways.[1,9] For example, CK1α is part of the destruction complex that targets β-catenin for ubiquitination and subsequent degradation in the absence of the Wnt ligand.[10] Following binding of the Wnt ligand to frizzled (Fzd), the Wnt co-receptor LRP5/6 is phosphorylated either by membrane-bound CK1γ (positive regulation)[11] or by CK1ε (negative regulation).[12] Furthermore, CK1δ and CK1ε phosphorylate axin and dishevelled (DVL) thereby causing a conformational

DOI: 10.1021/acs.jmedchem.8b00095
J. Med. Chem. 2018, 61, 4087−4102

change in the β-catenin destruction complex which prevents β-catenin from being degraded.[10a,13] In addition, Wnt-activation promotes recruitment of DDX3 to CK1ε, and their interaction directly stimulates CK1ε kinase activity, which in turn contributes to stabilization of β-catenin.[14]

Targeting Wnt signaling for therapeutic purposes is challenging due to its complexity and its role in a variety of developmental and homeostatic processes.[7] Currently, there are several compounds at different drug development stages able to modulate Wnt signaling.[15] Among these pharmacologically active substances used in preclinical settings, small-molecule inhibitors termed inhibitors of Wnt production (**IWPs**) have been reported.[16] **IWP** compounds, originally identified by screening of a synthetic chemical library, were able to block Wnt signaling by inhibiting porcupine (Porcn), a member of the membrane-bound O-acyltransferases (MBOAT) protein family. Palmitoylation of Wnt by Porcn is essential for Wnt secretion and signaling.[17,18] Consequently, inactivation of Porcn captures Wnt3A in the endoplasmic reticulum and, thus, leads to inhibition of Wnt signaling.[19] However, when used at higher concentrations, additionally to their inhibition of Porcn, **IWPs** have been shown to modify further events related to Wnt signaling. These include inhibition of phosphorylation of Lrp6 and Dvl2,[17] suggesting **IWPs** target related protein kinase activity.

Since **IWPs** show structural similarities to known CK1-specific benzimidazole inhibitors (e.g., 2-benzamido-*N*-(1*H*-benzo[d]imidazol-2-yl)thiazole-4-carboxamide,[20] (**Bischof-5**; Figure 1A–C), we hypothesized that **IWP** compounds could also inhibit CK1 isoforms. Thus, we performed docking studies of **IWPs** in the ATP binding pocket of CK1δ which revealed plausible binding modes (Figure 1D–E). To further prove this hypothesis, we performed *in vitro* kinase assays with different CK1 isoforms in the presence of commercially available **IWP** derivatives. Moreover, **IWP-2** was tested at a concentration of 1 μM in a panel of 320 kinases to determine a selectivity profile. Additionally, we could show that **IWP-2** and **IWP-4** were able to inhibit the proliferation of various CK1-dependent cancer cell lines, indicating their potential in cancer research and additionally in stem cell applications.

RESULTS

IWP Derivatives Inhibit the Activity of CK1δ. **IWP** small-molecule compounds have been reported to target Porcn by inhibition of palmitoyl transfer to Wnt proteins, a crucial modification for Wnt secretion.[21] Therefore, **IWP** compounds (in particular **IWP-2** and more recently **Wnt-C59**) have been routinely used as pharmacological tools to inhibit the Wnt pathway in various settings.[22] Since **IWPs** exhibit structural similarities to CK1-specific small-molecule inhibitors,[20,23] we became interested in analyzing their ability to inhibit CK1 isoforms. For this purpose, **IWP-2**, **IWP-2-V2**, **IWP-3**, and **IWP-4**[16] (Figure 2) were initially screened for their biological activities against different CK1 isoforms. Whereas full-length CK1δ, the C-terminal truncated form of CK1δ (CK1δKD), and CK1ε were inhibited by **IWP-2** and **IWP-4**, CK1α and CK1γ were only weakly affected. **IWP-2** inhibited full-length CK1δ to a 23% of residual activity, CK1δ KD to 19%, and CK1ε to 35%. IWP-4 inhibited full-length CK1δ to a 25% of residual activity, CK1δ KD to 22%, and CK1ε to 43%. In addition, **IWP-2-V2** and **IWP-3** did not inhibit CK1α, while inhibiting CK1γ3 and CK1ε only moderately. In contrast, the activity of both full-length CK1δ and CK1δKD were significantly reduced in these assays. Thus, our initial results suggested that the direct effects of **IWP** compounds on the Wnt pathway reported so far are not limited to the inhibition of Porcn, but may also affect CK1δ and/or CK1ε activity, respectively. We therefore aimed to analyze the biological impact of **IWPs** toward CK1δ and ε in more detail.

Next, IC_{50} values against rat GST wild-type CK1δ (^{wt}CK1δ), rat CK1δ KD, rat GST-CK1δ M82F (^{M82F}CK1δ, a typical "gatekeeper" mutation), and human ^{wt}CK1ε were determined by *in vitro* kinase assays using α-casein as substrate, CK1 isoforms as enzymes, and different concentrations of either **IWP-2**, **IWP-2-V2**, **IWP-3**, or **IWP-4** (Table 1, IC_{50} curves in Supplementary Figures 1 and 2). Herein, IC_{50} values of all four **IWP** derivatives against ^{wt}CK1δ were 4- to 7-fold lower than those against CK1ε. This CK1δ preference increased up to 17-fold when IC_{50} values against CK1δKD were compared to those against CK1ε (Table 1). The high degree of phosphorylation of ^{wt}CK1δ within its C-terminal domain, which is missing in CK1δKD, explains the 4-fold reduced IC_{50} value of CK1δKD and is in line with previous reports on the influence of the C-terminal domain on CK1 kinase activity.[20,24,25]

Table 1. Chemical Structures of IWP Compounds and their IC_{50} Values Against ^{wt}CK1δKD, ^{wt}CK1δ, ^{M82F}CK1δ, and ^{wt}CK1ε, Respectively[a]

Kinase	IC_{50} value (μM)			
	IWP-2	IWP-2-V2	IWP-3	IWP-4
	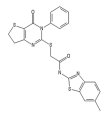	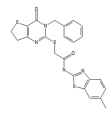	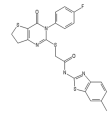	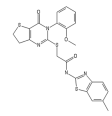
^{wt}CK1δ KD	0.32 ± 0.06	0.42 ± 0.06	0.55 ± 0.27	1.02 ± 0.13
GST-^{wt}CK1δ	0.93 ± 0.15	1.66 ± 0.37	1.89 ± 0.07	1.06 ± 0.18
GST-^{M82F}CK1δ	0.04 ± 0.01	0.06 ± 0.01	0.15 ± 0.03	0.14 ± 0.01
^{wt}CK1ε	4.03 ± 0.03	7.34 ± 2.58	>10	7.07 ± 2.01

[a] IC_{50} values were assayed as described in the Experimental Section using an inhibitor serial dilution, the respective kinase as enzyme, and α-casein as substrate. Values are expressed in micromolar units (μM) as mean of triplicate experiments ± standard deviation.

Interestingly, the gatekeeper mutant ^{M82F}CK1δ[25] was strongly blocked by all tested **IWPs** with IC_{50} values in the nanomolar range (Figure 3), suggesting a significant impact of the mutated phenylalanine residue toward ligand binding. Strikingly, **IWP-2-V2** showed an almost 28-fold increased inhibition of ^{M82F}CK1δ when compared to ^{wt}CK1δ. To analyze the role of ^{M82F}CK1δ in more detail, we docked **IWP-2-V2** both into the ATP-binding sites of a protein structure of ^{wt}CK1δ (PDB 4TW9)[24] and its gatekeeper ^{M82F}CK1δ mutant structure generated by homology modeling (Figure 4A–B). While the general binding poses in both kinases turned out to be quite similar, a focused analysis of ligand-protein interactions regarding gatekeeper residue 82 revealed significant lipophilic π-stacking interactions toward 82F in comparison to 82 M (Figure 4C–D). Thus, the high affinity of **IWP** compounds toward ^{M82F}CK1δ correlates with the modeled pose, further indicating a valid calculated binding mode.

DOI: 10.1021/acs.jmedchem.8b00095
J. Med. Chem. 2018, 61, 4087–4102

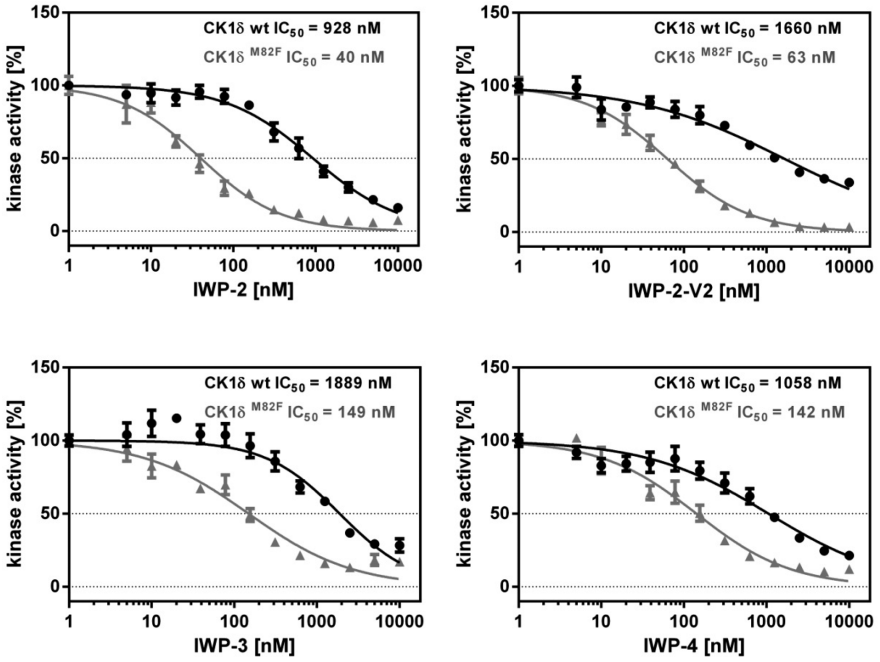

Figure 3. Differential inhibition of ^{wt}CK1δ and its gatekeeper mutant ^{M82F}CK1δ by **IWP** compounds. **IWP-2**, **IWP-2-V2**, **IWP-3**, and **IWP-4** were used to inhibit GST-^{wt}CK1δ or the GST-^{M82F}CK1δ gatekeeper mutant using *in vitro* kinase assays. Phosphate incorporation into α-casein was quantified by Cherenkov counting as described in the Experimental Section. Obtained data were normalized toward their correspondent DMSO control reactions. Error bars represent the standard error of the mean.

IWP Compounds Inhibit CK1δ in an ATP Competitive Manner. To investigate if **IWP** compounds were ATP-competitive inhibitors, **IWP-2** and its derivative **IWP-2-V2** were analyzed for their ability to inhibit GST-^{wt}CK1δ in the presence of different ATP concentrations (Figure 4E–F). While ATP concentrations increased, incorporation of ^{32}P labeled phosphate into α-casein decreased, indicating that both compounds act as ATP competitive inhibitors.

Selectivity Profiling of IWP-2 in a Panel of 320 Kinases Reveals CK1δ Selectivity. To characterize the selectivity of **IWP-2**, its inhibitor profile was measured in a panel of 320 protein kinases at concentrations of 0.1 μM and 1 μM (see Supplementary Table 1 and Figure 3A). Herein, at a concentration of 1 μM, only three kinases were identified to be moderately inhibited: CK1δ (55% of residual activity), TLK2 (59%), and ZAP70 (54%). Interestingly, besides CK1δ, no further CK1 family members or their paralogs were significantly inhibited (see Supplementary Figure 3B). To confirm the inhibitory effect of **IWP-2** as suggested by the profiling, we carried out in-house enzymatic kinase assays using TLK2 and ZAP70 as enzymes. In contrast to the panel data, we could not confirm the inhibitory effects of **IWP-2** on TLK2 and ZAP70 in the tested range of **IWP-2** concentrations (see Supplementary Figure 3E–F). Thus, these results indicate that **IWP-2** seems to be specific for CK1δ kinase inhibition.

Binding Mode of IWP-2 in CK1δ – Parameters Triggering CK1 Isoform Specificity. Based on the high CK1δ specificity as indicated by the profiling, we became interested in further proving the modeled molecular binding mode of **IWP-2** in the active site of CK1δ (see Figure 1). Hence, we aimed to elucidate a structure of **IWP-2**/CK1δ ligand-protein complex by X-ray crystallography. Crystals were obtained by co-crystallization of a truncated version of CK1δ (tCK1δ) with **IWP-2**, which diffracted to a resolution of 2.1 Å. The asymmetric unit contains four molecules of CK1δ, which are all structurally very similar (RMSD of backbone alignment: 0.438–0.991 Å for at least 272 residues). In line with kinetic data and docking results shown above, in the crystal structure we identified the ATP binding pocket as a binding site for **IWP-2** (Figure 5 and Supplementary Table 2 and Figure 4). As predicted by the modeling, the ligand is hydrogen bonded involving its amide group and the benzothiazole moiety to the main chain of the hinge region. In more detail, binding of **IWP-2** in CK1δ is further stabilized by numerous van der Waals interactions between the benzothiazole moiety and side chain residues Ile23 and Leu85. More importantly, the benzothiazole moiety also interacts with the gatekeeper residue Met82 resulting in a significant rearrangement of the Met82 side chain compared to inhibitor-free CK1δ. As a consequence, the side chain of Ile68 is rotated by 180° which in turn may probably be one important factor for the isoform selectivity of **IWP-2**. Rotation of Ile68 is mainly restricted by steric clashes with the side chain of Met80 in CK1δ. In comparison, in CK1α the rotation of the corresponding Ile76 is typically limited by steric hindrance with the side chain residue of Leu88. The diastereotopic methyl groups of Leu88 hold the δ-methyl group of Ile76 in its position and might prevent rotation of Ile76 to a greater extent compared to Met80 in CK1δ upon **IWP-2** binding. Furthermore, CK1α exhibits a tyrosine (Tyr79) in proximity to Ile76, whereas CK1δ exhibits only a cysteine (Cys71) at this position, thus giving Met80 more conformational freedom compared to Leu88. As a consequence, it is likely that Ile68 is able to rotate with lower energy barrier in CK1δ compared to Ile76 in CK1α, thus favoring **IWP-2** binding in CK1δ. Mutation of the Met82 to phenylalanine may not only lead to tighter interactions between **IWP-2** and CK1δ (as described above) but also might remove the residual steric clashes arising from the conformational changes of Met82.

Based on the data obtained for **IWP-2**/CK1δ ligand-protein complex, we speculate that the C-terminal extensions of CK1δ

DOI: 10.1021/acs.jmedchem.8b00095
J. Med. Chem. 2018, 61, 4087–4102

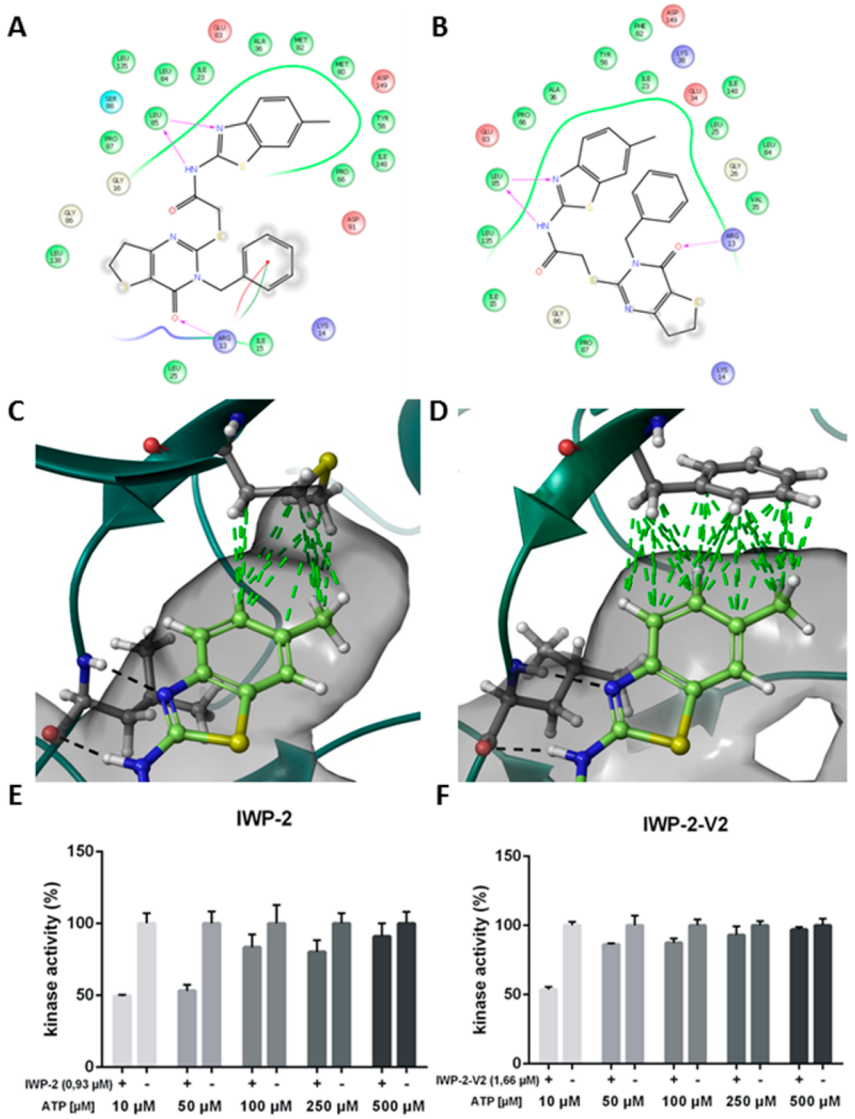

Figure 4. Modeled binding modes of **IWP-2-V2** in ^{wt}CK1δ (A) and in a homology model of ^{M82F}CK1δ (B) presented as 2D ligand-interaction diagram (LID). Protein structures are based on PDB 4TWC,[1] respectively. Poses were determined by docking the ligands into the active site of structures (Glide, Schrödinger LCC, NY). Key hydrogen-bond interactions of the benzothiazole moiety toward Hinge Leu85 are shown. Focus on lipophilic interactions (green dotted lines) of the benzothiazole moiety of **IWP-2-V2** toward gatekeeper residue ^{wt}CK1δ (Met, C) and ^{M82F}CK1δ (Phe, D) in the hydrophobic pocket I. The phenylalanine residue in the ^{M82F}CK1δ mutant forms significant π-stacking interactions when compared to ^{wt}CK1δ. (E and F) The potential of **IWP-2** and **IWP-2-V2** to inhibit the kinase activity of GST- ^{wt}CK1δ was assayed in *in vitro* kinase assays in the presence of increasing ATP concentrations (10, 50, 100, 250, and 500 μM) to demonstrate the ATP competitive properties of this compound. **IWP-2** was used at its determined IC_{50} concentration of 0.93 μM for GST-^{wt}CK1δ and **IWP-2-V2** at its IC_{50} concentration of 1.66 μM. α-Casein was used as a substrate and DMSO in control reactions. Results are shown as normalized bar graphs.

compared to CK1ε isoform may contribute to **IWP-2** binding since there is a remarkable difference in the susceptibility of ^{wt}CK1δ KD and GST-^{wt}CK1δ toward **IWP-2** inhibition (as shown in Table 1). Noteworthy, when redocking **IWP-2** into the newly generated CK1 structure, the binding pose determined by X-ray analysis could be reproduced.

IWPs Inhibit the Proliferation of Cancer Cell Lines. We next performed cell viability assays to determine EC_{50} values of **IWP** compounds for eight selected established tumor cell lines (Table 2 and Supplementary Figures 5−7). Herein, **IWP-2**, **IWP-2-V2**, and **IWP-3** inhibit the proliferation of the investigated cell lines within the single digit μM range. In contrast, **IWP-4** consistently inhibited cell proliferation in all tested cell lines with EC_{50} values even in the sub-μM range. For example, while the EC_{50} value obtained for **IWP-2** on MiaPaCa2 cells was 1.90 μM, **IWP-4** was approximately 10-fold more effective (EC_{50} value 0.23 μM).

Effect of IWP-2 on Kinase Activity in Panc-1 Cells. In order to analyze whether **IWP-2** has an impact on intracellular CK1 kinase activity, we selected CK1-dependent Panc-1 cells[26] for further experiments. Panc-1 cells were either untreated or treated with 2.33 μM **IWP-2** for 48 h. Following incubation, cells were lysed, and lysates were subsequently fractionated via an anion exchange column (as described in the Experimental Section). Herein, CK1δ kinase activity was determined using GST-p53$^{1-64}$ (FP267) as a substrate, and fractions were used as enzyme sources for *in vitro* kinase assays. In **IWP-2** treated cells, the CK1δ kinase peak activity was reduced to approximately 66% residual activity compared to the activity in untreated cells, respectively (Figure 6A). Furthermore, *in*

DOI: 10.1021/acs.jmedchem.8b00095
J. Med. Chem. 2018, 61, 4087−4102

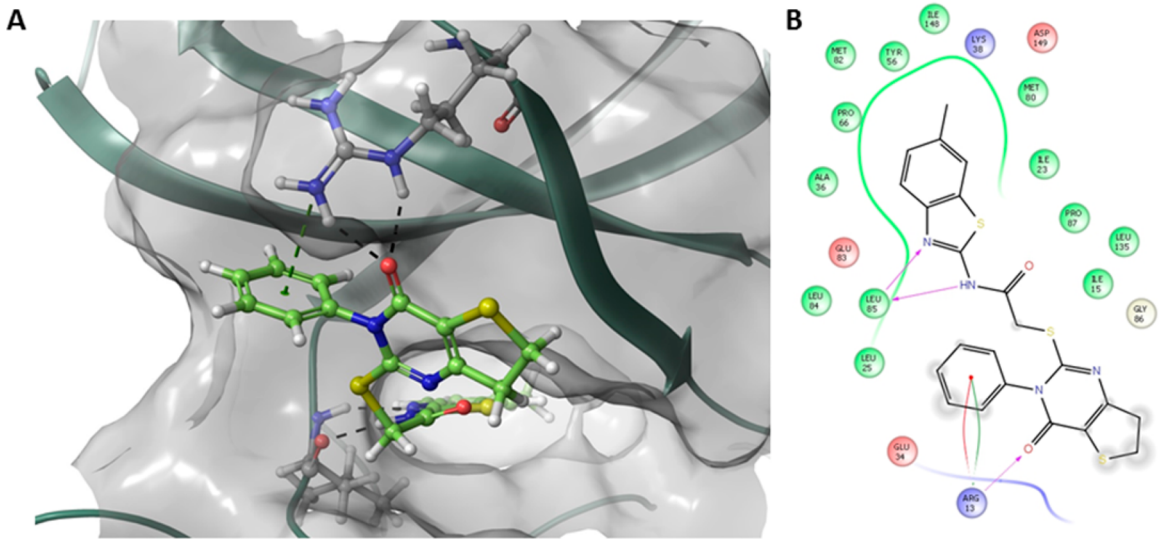

Figure 5. Binding mode of **IWP-2** in CK1δ as determined by X-ray analysis. (A) Pose of **IWP-2** in the ATP binding site of CK1δ showing the Connolly surface. (B) Corresponding LID with the main hydrogen-bond interactions toward Hinge residue Leu85. More details in the SI.

Table 2. IWPs Strongly Inhibit Cell Proliferation of Various Cancer Cell Lines[a]

cell line	IWP-2	IWP-2-V2	IWP-3	IWP-4
A818-6	8.96 ± 2.49	>10	>10	0.93 ± 0.07
MiaPaCa2	1.90 ± 0.43	5.65 ± 0.16	5.34 ± 0.49	0.23 ± 0.01
Panc-1	2.33 ± 0.22	>10	4.87 ± 1.03	0.23 ± 0.02
Panc-89	3.86 ± 0.54	3.10 ± 0.70	5.07 ± 0.37	0.58 ± 0.12
HT29	4.67 ± 1.59	>10	>10	0.34 ± 0.10
HEK293	2.76 ± 0.65	>10	3.50 ± 0,51	0.28 ± 0.05
SW620	1.90 ± 0.28	8.52 ± 0,13	8.62 ± 0.84	0.23 ± 0.01
Capan	2.05 ± 0.44	>10	>10	0.23 ± 0.01

[a] EC_{50} values were determined for **IWP-2**, **IWP-2-V2**, **IWP-3**, and **IWP-4** in eight tumor cell lines as described in the Experimental Section using serial inhibitor dilutions in each case. **IWP-4** consistently reduced the cell proliferation in different cell lines in the nanomolar range. Values are expressed in micromolar units (μM). DMSO-treated cells were used as a control.

vitro kinase assays in the presence and absence of control CK1δ inhibitors, **IC261**[27a] and **PF670462**,[27b] revealed a reduction of kinase activity in the kinase peak fraction by approximately 40%, providing further evidence for the presence of CK1δ in the kinase peak fraction (Figure 6 B). Thus, our results suggest that **IWP-2** reduces the activity of CK1δ in Panc1 cells. In a more general context, inhibition of Wnt signaling by **IWP** compounds used at μM concentrations may not be exclusively affecting their known target Porcn but could additionally result in CK1δ inhibition. These findings have substantial implications on **IWP**-mediated inhibition in various studies of proliferation of tumor cells and within stem cell biology, respectively. **IWP** derivatives are commonly used in modern stem cell protocols for the generation of human induced pluripotent stem cell (hiPSC)-derived cardiomyocytes[28−30] or in the conversion of mouse embryonic stem cells (ES) to epiblast-like stem cells[31] at concentrations of 5 μM, a concentration corresponding to the EC_{50} values of **IWPs** for effective cellular CK1δ inhibition.

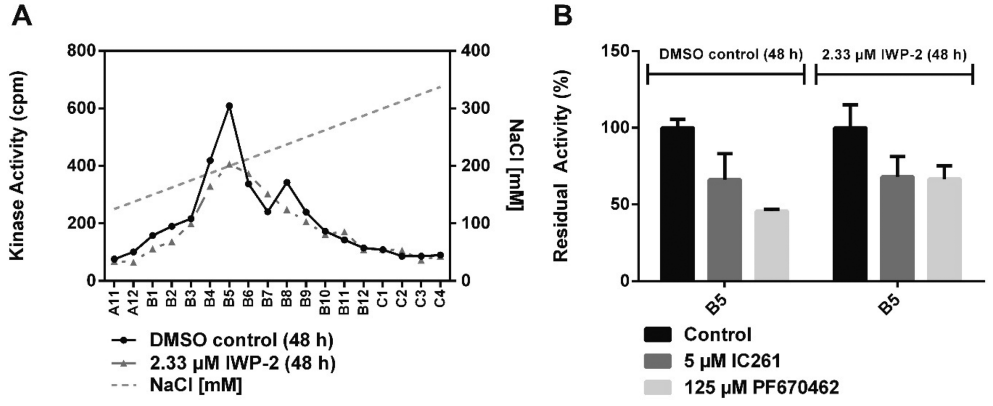

Figure 6. CK1δ kinase activity in untreated and **IWP-2** treated Panc1 cells. (A) Panc1 cells were either treated with DMSO (control) or with **IWP-2** for 48 h and were then lysed and fractionated on an anion exchange column. Thereafter, *in vitro* kinase assays were performed of single fractions using GST-$p53^{1-64}$ as substrate. ^{32}P phosphate incorporation was quantified by Cherenkov counting. (B) Fraction B5 was further analyzed by performing *in vitro* kinase assays using CK1δ inhibitors **IC261** and **PF670462** to confirm the presence of CK1δ in this fraction. All values were normalized to their respective DMSO control.

DOI: 10.1021/acs.jmedchem.8b00095
J. Med. Chem. 2018, 61, 4087−4102

Scheme 1. Overview of the Synthetic Route Towards IWP-Based Derivatives 17−23 Showing Variability at the Aryl System Substituted at the Tetrahydrothieno-Pyrimidinone Core[a]

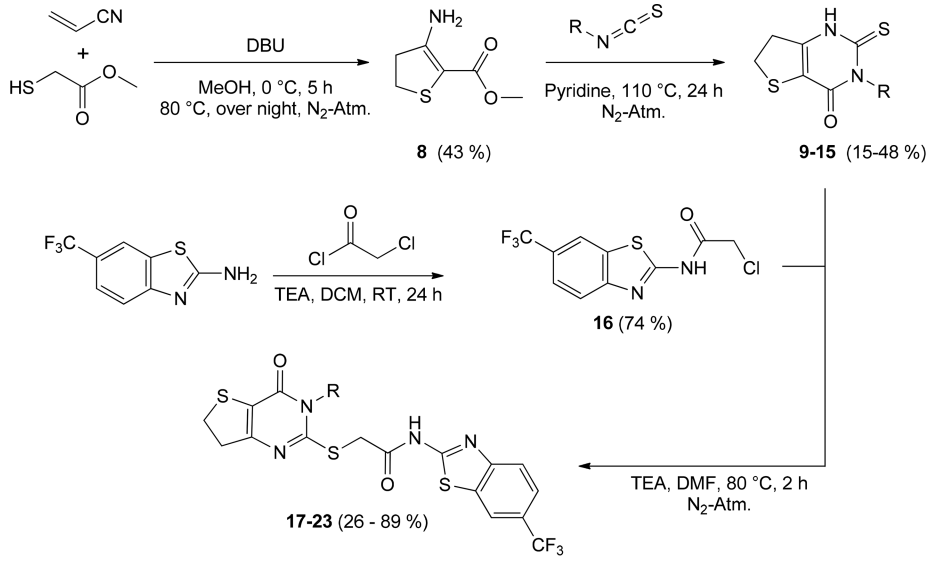

Compound #	R =
17	
18	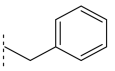
19	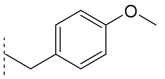
20	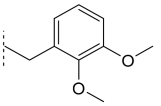
21	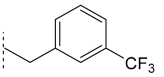
22	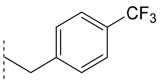
23	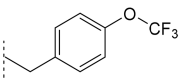

[a]Details can be found in the Experimental Section and SI.

Design and Synthesis of Novel IWP-Derived CK1δ Inhibitors. Based on the data obtained so far, we set out to optimize **IWP** hit compounds toward potent, specific, and effective CK1δ/ε inhibitors. We aimed to establish a flexible synthetic route to produce modified **IWP**-derived compounds for the generation of initial CK1-targeted structure−activity relationships (SAR). Thus, the original synthesis of **IWP** compounds was adapted (Scheme 1). Herein, a convergent strategy was followed coupling a benzothiazole[32] building block (**16**) with substituted tetrahydrothieno-pyrimidinones[16] (**9**−**15**) to yield test compounds **17**−**23**.

In order to enhance ligand-protein interactions toward the hydrophobic pocket I, and accordingly to the substitution pattern in benzimidazole CK1δ inhibitor **Bischof-5**[3] (see Figure 1) and further related CK1 inhibitors,[23] we introduced a trifluoromethyl group to the **IWP** benzothiazole scaffold. Besides this slight modification, we decided to initially keep the 2-amido-benzothiazole core as it was shown to mediate bidentate hinge binding and, at the same time, quite optimally fit into the hydrophobic pocket I of CK1δ. In contrast to maintaining the 2-amido-benzothiazole scaffold, we focused on variations of the phenyl- and benzyl moiety attached to the

DOI: 10.1021/acs.jmedchem.8b00095
J. Med. Chem. 2018, 61, 4087−4102

tetrahydrothieno-pyrimidinone core, respectively. In line with our modeling and X-ray analysis of **IWP-2** in CK1δ (Figure 5), this part of the inhibitors was found to address the solvent-exposed hydrophobic region II. Thus, we designed a small set of compounds with variability at the aryl system attached to the tetrahydrothieno-pyrimidinone core (**17**−**23**, Scheme 1). Modeling of these compounds in the active site of CK1δ indicated plausible binding modes. However, within this preliminary set, it was not possible to prioritize any compound since all ligands were calculated to have very similar docking scores. Thus, we decided to prepare this small set of compounds for subsequent initial determination of SAR. Synthetically, modifications were readily introduced by using substituted isothiocyanate precursors (**2**, **4**, **5**, **6**, and **7**, Scheme 1 and SI) during the pyrimidinone ring closure reaction.

Next, we determined IC_{50} values of these new test compounds against rat ^{wt}CK1δ KD, rat ^{wt}GST-CK1δ, rat GST-^{M82F}CK1δ, and human ^{wt}CK1ε by *in vitro* kinase assays using α-casein as substrate (Table 3, and Supplementary Figures 9−11). According to the design concept regarding lipophilic interactions toward hydrophobic region II, the compounds were shown in general to have modestly increased binding affinity to their targets. Given only minor variations in substitution patterns for all compounds, the gain in affinity turned out to be within a similar range. When compared to **IWP-2**, compound **19** was determined to have approximately 2-fold higher affinity for CK1δ (IC_{50} = 0.41 μM). To further characterize CK1 isoform specificity of these derivatives, they were assayed at a concentration of 1 μM against GST-CK1α and GST-CK1γ3. Herein, all compounds showed no significant inhibition, indicating selectively toward CK1 isoforms δ and ε (see Supplementary Figure 12).

Table 3. Inhibitory Activity of Test Compounds 17−23 against ^{wt}CK1δKD, ^{wt}CK1δ, ^{M82F}CK1δ, and ^{wt}CK1ε, Respectively[a]

compound	^{wt}CK1δ KD	GST-^{wt}CK1δ	GST-^{M82F}CK1δ	^{wt}CK1ε
17	0.40 ± 0.09	0.66 ± 0.08	0.21 ± 0.03	4.12 ± 0.80
18	0.52 ± 0.04	1.06 ± 0.13	0.27 ± 0.02	1.41 ± 0.29
19	0.09 ± 0.02	0.41 ± 0.02	0.09 ± 0.01	0.56 ± 0.09
20	0.23 ± 0.02	0.76 ± 0.21	0.21 ± 0.03	1.23 ± 0.53
21	n.d.	1.03 ± 0.36	n.d.	n.d.
22	n.d.	0.33 ± 0.07	n.d.	n.d.
23	n.d.	0.70 ± 0.17	n.d.	n.d.

[a] IC_{50} values were assayed as described in the Experimental Section using an inhibitor serial dilution, the respective kinase as enzyme and α-casein as substrate. Values are expressed in micromolar units (μM) as mean of triplicate experiments ± standard deviation. DMSO was used as a control. Abbreviations: n.d.: not determined.

To judge the structural impact of these modifications toward kinase selectivity, we selected compound **19** for further profiling in a panel of 320 kinases (see Supplementary Figure 3A−D and Table 1). By this screen, compound **19** was determined to be selective for CK1δ at a concentration of 1 μM which is comparable to the selectivity profile of **IWP-2**. However, selectivity profiling of **19** at 10 μM revealed a wealth of other inhibited kinases (see Supplementary Table 1 and Figure 3A−B). Since the CK1 inhibition of **19** (IC_{50} = 0.41 μM) was slightly improved compared to that of the original hit compound **IWP-2** (IC_{50} = 0.93 μM), we next determined their effects on Wnt signaling in cellular settings also using relevant sub-μM concentrations.

Novel IWP Derivatives Exhibit Distinct Profiles on Wnt/β-Catenin Signaling. Functional perturbation of canonical Wnt signaling by **IWP-2** and its derivative **19** was probed in two specific cell-based assay setups to discriminate between a porcupine-dependent and porcupine-independent mode-of-action.[4c] HEK293T cells were transiently transfected with a 7-tandem-repeat of TCF/LEF response elements (i.e., SuperTOPFlash vector), and Wnt signaling was activated by exogenous addition of Wnt3A-containing conditioned medium from mouse L-cells (i.e., paracrine pathway activation) or by autologous expression of Wnt3A from a co-transfected Wnt3A expression vector (i.e., autocrine and paracrine pathway activation).[33,34] The latter assay setup strongly depends on the cells' capacity to post-translationally process Wnt3A by the action of porcupine to secrete mature ligands for functional pathway activation. The data showed that all **IWP**-type Wnt inhibitors inhibited porcupine-dependent canonical Wnt signaling in this setup (Figure 7A). **Wnt-C59**[35] is among the most potent currently reported porcupine inhibitors[36] and served as

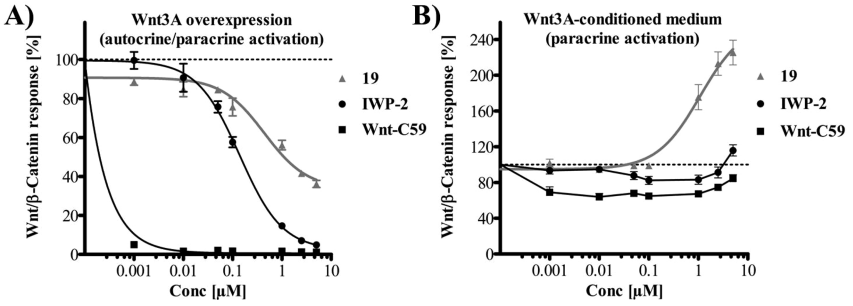

Compd	IC_{50} [µM]	$I_{max\ (5\ µM)}$ [%]
19	0.71 ± 0.38	38.8 ± 2.0
IWP-2	0.157 ± 0.03	5.5 ± 0.3
Wnt-C59	< 0.001	1.1 ± 0.2

Compd	EC_{50} [µM]	$E_{max\ (5\ µM)}$ [%]
19	1.47 ± 0.55	225 ± 14
IWP-2	n.a.	n.a.
Wnt-C59	n.a.	n.a.

Figure 7. Perturbation of Wnt/β-catenin signaling by IWP derivatives **19**, **IWP-2**, and **Wnt-C59** in a Wnt reporter gene assay. (A) Porcupine-dependent Wnt signaling upon Wnt3A overexpression represents autocrine/paracrine pathway stimulation. (B) Porcupine-independent Wnt signaling upon addition of Wnt3A-conditioned medium represents paracrine pathway stimulation. HEK293T cells were transfected with a 7x-TCF/LEF-firefly luciferase vector (SuperTOPFlash), *Renilla* luciferase vector for normalization and luciferase activity was measured after 22 h of compound exposure. Data derived from at least n = 2 independent experiments, with DMSO as the control (= 100%).

DOI: 10.1021/acs.jmedchem.8b00095
J. Med. Chem. 2018, 61, 4087−4102

a positive control (IC_{50} < 1 nM), while **IWP-2** and **19** had IC_{50}'s of 0.157 μM and 0.71 μM, respectively.

Strikingly, both **IWP-2** and **Wnt-C59** did not show dose-dependent inhibition when the signaling cascade was activated by exogenous Wnt3A (Figure 7B), whereas **19** appeared to synergize with Wnt3A and thus further activated canonical signaling. At first, this finding was somewhat surprising and required further validation concerning possible assay artifacts. For instance, it is well-known that 2-aminobenzothiazoles, such as **IWP-2** and probably **19**, too, can potentially show unspecific reporter gene activation through inhibitor-based stabilization of luciferases.[37] Thus, we considered this possibility by cotransfection of a constitutively active *Renilla* luciferase reporter in all experiments. Indeed, a characteristic low-level reporter activation was observed up to 1.3-fold and 1.5-fold of the baseline Wnt activity in the autocrine/paracrine and paracrine assay setup, respectively (see Figure 7). However, this basal unspecific activity is taken into account by normalization of firefly by *Renilla* luciferase activity. It should also be noted that compound/scaffold-dependent effects on distinct proliferation rates are considered by this method. Moreover, compound exposure in a time-dependent manner (6 h and 22 h) in cell viability assays complemented this data (see Supplementary Figures 13 and 14).

The off-target activity of the herein reported IWP derivative **19** on CK1 isoforms results in a unique profile on canonical Wnt signaling. It is well-known that different CK1 isoforms fulfill diverse roles within the signaling cascade, depending on the temporal and tissue-specific regulation of the actual pathway.[9] In fact, pathway synergy or stimulation can be explained by an underlying inhibitory activity on CK1δ isoforms. It has been shown that CK1δ phosphorylates the Wnt-dependent transcription factor Lef1, thereby inhibiting its binding interaction with β-catenin. Thus, inhibition of this inhibitory effect on canonical signaling results in pathway stimulation.[38] In this context, **IWP-2**'s lack of activity in the paracrine assay setup is likely due to its ca. 10-fold less potent CK1δ inhibition compared to **19** (Tables 1 and 3), while porcupine inhibition cannot be effective at all. On the other hand, **19**'s Wnt3A synergy appears to be overridden by still effective porcupine inhibition in the autocrine/paracrine assay setup, thus explaining the modest inhibitory activity of **19** (IC_{50} = 0.71 μM) in this setup compared to the parent **IWP-2** (IC_{50} = 0.157 μM). Notably, profiling of two different chemotypes of CK1δ/ε inhibitors, that is, SR-3029 and PF-670462, raises questions whether the observed activity of **19** is solely due to a unique inhibition profile of CK1 isoforms or a consequence of an additional off-target (see Supplementary Figure 14). SR-3029 showed dose-dependent Wnt/β-catenin inhibition up to 0.1 μM in both assay setups while being toxic at higher concentrations. Another explanation could be differences in the subcellular distribution and cellular target engagement of these three unrelated chemotypes of CK1δ/ε inhibitors. Additional studies are required to decipher compound **19**'s activity as a Wnt signaling modulator.

Taken together, these data underline the utility of the herein presented **IWP** derivatives as novel pharmacological tools for CK1δ-dependent Wnt/β-catenin perturbation in different cellular, tissue, and disease context. However, for future projects, it would be desirable to eliminate any remaining activity on porcupine while keeping (and improving) CK1δ/ε inhibition of these compounds.

DISCUSSION AND CONCLUSIONS

IWP-2 and its derivatives have been initially described to be potent Wnt pathway inhibitors,[17] a discovery that has led to extensive use of **IWP-2** in biological research applications studying this highly complex signaling process. **IWPs** effectively block the secretion of Wnt ligands by inhibiting Porcn, a membrane-bound O-acyltransferase catalyzing the palmitoylation of Wnt. However, in our current project, we have found that **IWP** compounds also inhibit CK1δ/ε *in vitro* and cell culture, adding a new layer of complexity to the effects of these small molecules on the Wnt pathway.

Initial screenings were performed using different **IWP** derivatives at 10 μM on the isoforms of CK1 α, γ3, δ (in its full form and kinase-domain-only form) and CK1ε (Figure 1). CK1δ was consistently inhibited at various extents by the **IWP** derivatives, while CK1ε was more weakly blocked despite its structural similarity to CK1δ. In contrast, the tested **IWPs** showed low affinities to CK1γ3 and CK1α which were thus mostly unaffected by any of the treatments (Figure 1 and Supplementary Data). Additionally, we provide structural evidence by determining a complex of **IWP-2** in CK1δ (X-ray crystallography). Furthermore, the selectivity profiling of **IWP-2** in a panel of 320 kinases demonstrated its preference for CK1δ. Moreover, **IWP-2** was shown to inhibit the ^{M82F}CKδ gatekeeper mutant with an IC_{50} even in the nanomolar range (Figure 3). Typically, small-molecule kinase inhibitors show a higher capability to inhibit wild-type kinases, rather than mutant forms.[39] To the best of our knowledge, this is the first report of **IWPs** inhibiting protein kinases as targets. Finally, we started to reveal preliminary SAR to optimize the **IWP** scaffold toward isoform-specific CK1 inhibitors.

In summary, we characterized **IWP** derivatives as small-molecule CK1 isoform-specific agents suggesting that some effects of prior **IWP** applications as Wnt inhibitors may be not be limited to their known target Porcn. The presented data render **IWPs** as interesting hits for the development of novel potent, specific, and effective CK1δ/ε inhibitors. Compound **19** will serve as starting point toward further optimized derivatives as novel pharmacological tools to study CK1-dependent processes in cancer and stem cell research.

EXPERIMENTAL SECTION

Commercially Available Chemical Compounds and Enzymes. Inhibitors of Wnt Production **IWP-2**, **IWP-2-V2**, **IWP-3**, and **IWP-4** were purchased from Cayman Chemical (Ann Arbor, MI, USA) and were diluted in DMSO (GIBCO, Karlsruhe, Germany). α-Casein and poly(L-glutamic acid-L-tyrosine) were acquired from Sigma-Aldrich (St. Louis, MO, USA), rat recombinant CK1δ kinase domain (KD) from New England Biolabs, (NEB, Frankfurt am Main, Germany), and human CK1ε from Invitrogen (Karlsruhe, Germany). TLK2 and ZAP70 were obtained from ProQinase (Freiburg, Germany).

Plasmids. For the expression of wild-type (wt) bovine CK1α, the plasmid pGEX-2T-CK1α (FP296) was used. Human CK1γ3 was expressed using the plasmid pGEX-2T-CK1γ3 (FP1054).[40] Expression of wild-type rat CK1δ and its gatekeeper mutant was carried out using pGEX-2T-^{wt}CK1δ (FP449)[41] and pGEX-2T-^{M82F}CK1δ (FP1153),[28] respectively. The GST-p53$^{1-64}$ fusion protein was expressed using pGEX-2T-p53$^{1-64}$ (FP267), and used as substrate. Expression and purification of the GST-fusion proteins were carried out previously described.[42] A C-terminally truncated construct (tCK1δ) encoding amino acids 1−294 in a codon-optimized version for expression in *E. coli* was ordered from Geneart (Thermofisher, Germany) and cloned into the NdeI and XhoI sites of the pET28a vector, resulting in an N-terminally hexa-histidine tagged protein with a thrombin site to cleave

DOI: 10.1021/acs.jmedchem.8b00095
J. Med. Chem. 2018, 61, 4087−4102

off the tag. Wnt/β-Catenin reporter assays were performed with the following commercially available vectors: M50 Super 8x TOPFlash (Addgene Plasmid 12456) coding for firefly luciferase under control of TCF/LEF binding region (7 repeats), TK-driven pRL *Renilla* luciferase control reporter vector (Promega Cat # E2241) and Wnt3a cDNA in pUSEamp (Upstate Biotech, Cat # 21−124).

***In Vitro* Kinase Assays.** *In vitro* kinase assays were performed with different CK1 isoforms and **IWP** derivatives at an ATP concentration of 10 μM and using DMSO controls as described previously.[43,44] Where indicated, higher ATP concentrations (50, 100, 250, and 500 μM) were used. Bovine GST-CK1α (FP296), rat recombinant CK1δ kinase domain (CK1δKD), rat GST-^{wt}CK1δ (FP449), rat GST-^{M82F}CK1δ (FP1153), recombinant human CK1ε, TLK2, and ZAP70 were used as sources of enzyme. Phosphorylated proteins were separated by SDS-PAGE and stained with Coomassie. α-Casein served as a substrate for most kinase assay reactions. Kinase assays performed with ZAP70 were done using poly(L-glutamic acid-L-tyrosine) as substrate. Phosphate incorporation was detected by autoradiography of dried gels. The phosphorylated protein bands were cut out and quantified by Cherenkov counting. Dose−response analyses were carried out using GraphPad Prism 6 (GraphPad Software, Inc., La Jolla CA, USA) statistical software.

High-Throughput Kinase Profiling. The residual activity of 320 eukaryotic kinases was measured by ProQinase GmbH (Freiburg, Germany) in the presence of compounds **IWP-2** and **19** (1 μM). Dendrograms illustrating the phylogenetic relations of the kinases were generated using TREEspotTM Software Tool Image and reprinted with permission from KINOMEscan, a division of DiscoveRx Corp., Discoverx Corporation 2010.

Cell Lines. The pancreatic cancer cell lines MiaPaCa,[45] Panc1,[46] the human embryonic kidney cell line HEK293[47] were grown in Dulbecco's modified Eagle's medium (DMEM). The human colon adenocarcinoma cell line HT29[48] was grown in McCoy's 5A medium. The pancreatic cancer cell line Panc89[49] was grown in DMEM:RPMI (1:1) medium. The cell line[50] Capan1, also of pancreatic origin, was grown in RPMI medium. The colorectal adenocarcinoma cell line SW620[51] was grown in Leibovitz L-15 medium. All media were supplemented with 10% fetal calf serum (FCS; Biochrom, Berlin, Germany), 100 units/mL penicillin, 100 μg/mL streptomycin (Gibco, Karlsruhe, Germany), and 2 mM glutamine. All cells were cultured at 37 °C in a humidified 5% carbon dioxide atmosphere. HEK293T cell line was kindly provided by the Max Planck Institute of Molecular Physiology (Dortmund, Germany). These cells cultured in DMEM supplemented with 10% FCS.

Cell Viability Assay. Cells were seeded at a concentration of 5 × 10^4 cells/mL in 96-well cell culture plates and allowed to attach overnight at 37 °C and 5% CO_2. To investigate the effects of compounds on cancer cell proliferation, cells were treated with various concentrations (ranging from 0.313 μM to 10 μM) of inhibitor, with untreated and DMSO-treated cells serving as a control. After an incubation period of 48 h at 37 °C, 10 μL of a MTT (3-(4,5-dimethylthiazol-2-yl)-2,5-diphenyltetrazolium bromide) 12 mM solution in PBS were added, followed by further incubation for 4 h at 37 °C. Media containing MTT was then removed carefully, and 100 μL of 0.04 N HCl in isopropanol was added. To dissolve the formazan crystals, the plates were placed for 30 min on an orbital shaker. The resulting purple solution was spectrophotometrically measured at 570 nm. Experiments were repeated at least three times with four replicates per assay.

Fractionation of Cell Extracts by FPLC. **IWP-2**-treated (EC_{50} = 2,33 μM) and DMSO-treated Panc1 cells were lysed in sucrose lysis buffer. Total protein extract (1.4 mg) was diluted in prefiltered FPLC buffer A (50 mM Tris−HCl pH 7.5, 1 mM EDTA, 1 mM EGTA, 5% (v/v) glycerol, 0.03% (v/v) Brij-35, 1 mM benzamidine, 25 μg/mL aprotinin, 0.1% (v/v) β-mercaptoethanol). Cell lysates were then passed through a 0.45 μm filter and injected into an anion exchange column (Resource Q; GE Healthcare UK) attached to an EttanLC FPLC system (GE Healthcare, UK). Proteins bound to the cationic surfaces of the column were eluted with a linear ascending NaCl gradient by gradually increasing percentage of FPLC buffer B (equal to buffer A plus 1 M NaCl). Fractions of 250 μL volume were collected. Three μL from selected protein fractions were used for *in vitro* kinase assays, as described above, to determine CK1-specific kinase activity. To confirm CK1 in the peak fraction, kinase assays were repeated in the presence of given concentrations of CK1δ-specific inhibitors IC261 and PF670462. DMSO was used as a control and GST-p53$^{1-64}$ as substrate.

Dual Luciferase Reporter Gene Assay. The assay was performed as described previously.[10b,33] Briefly, compounds were tested in HEK293T cells in a 96-well plate format. For transient transfection, Lipofectamine2000 (Thermo Fisher) and plasmids were pre-incubated in Opti-MEM medium for 15 min at room temperature. For the autocrine/paracrine assay setup, 3 × 10^6 cells (for one 96-well plate) were transfected with the Wnt3A-expressing vector and the Super(8x)TOPflash reporter vector together with the TK-*Renilla* luciferase control vector for internal luminescence normalization purposes, followed by incubation for 8 h. Transfected cells were harvested and seeded on 96-well plates in 110 μL media at 25,000 cells per well and allowed to adhere for 1 h. Cells were treated either with 10 μL of compound dilution (final concentrations 5, 2.5, 1, 0.5, 0.1, 0.05, 0.01, 0.001, 0.001 μM with 0.5% DMSO) or DMSO (0.5%) as the vehicle controls. For paracrine pathway activation, cells were stimulated by addition of Wnt3A-conditioned medium that was freshly harvested from mouse L-cells overexpressing the Wnt protein (L-Wnt3A).[52] Control cells were treated with L-cell medium. Transfection of cells was done with the same vectors as described above, except for the Wnt3A-expressing vector. Cells were seeded in 80 μL and 25,000 cells/well 12 h post-transfection before stimulation with 30 μL of Wnt3A-conditioned medium. Compound treatment was conducted as described above. After 22 h incubation, the medium was carefully aspirated and both luciferase activities measured using the Dual-GloLuciferase Assay System (Promega) according to the manufacturer's protocol on a Tecan-Infinite 200 Plate Reader. Data were processed by normalizing Firefly with *Renilla* luciferase signals from each well. Each condition was repeated in technical triplicates with at least two independent biological replicates. EC_{50} and IC_{50} values were calculated by nonlinear regression analysis using the GraphPad Prism 5 software (version 5.03).

Molecular Modeling. Molecular modeling was performed on a DELL 4 core system. For visualization Maestro, version 10.3, Schrödinger, LLC, (New York, NY, USA, 2014) was used. Protein crystal structures were prepared prior to docking by the Protein Preparation Wizard using default settings. The X-ray crystal structure refinement process included the addition of hydrogen atoms, optimization of hydrogen bonds, and removal of atomic clashes. Missing side chains and loops were filled in. Furthermore, selenomethionines were converted to methionines, and water molecules were deleted.

Small-molecule ligands were prepared to create energetically minimized 3D geometries and assign proper bond orders (MacroModel). Accessible tautomer and ionization states were calculated prior to screening (LigPrep). To generate bioactive conformers, a conformational search method was used (ConfGen). Receptor grid generation was performed by Glide. For ligand docking, the Glide SP workflow was used (default settings). Energetically minimized ligand conformations were docked into the active site of the protein; possible binding poses were determined and subsequently ranked based on their calculated docking score.

Chemistry. All chemical reagents were commercially available and were used without further purification from abcr GmbH, Karlsruhe, Germany; Sigma-Aldrich Chemie GmbH, Merck Group, Munich, Germany; Merck Millipore, Darmstadt, Germany; Acros Organics, Thermo Fisher Scientific, Geel, Belgium. Infrared spectra (IR) were recorded on a Shimadzu IRAffinity-1S FTIR-spectrometer. NMR spectra were recorded on a Bruker Avance III 300 spectrometer (300 MHz ^{1}H frequency), (75 MHz ^{13}C NMR frequency). Chemical shifts are reported in ppm, multiplicity, and coupling constant *J* (Hz). Spectra were referenced to internal DMSO-d_6 or internal $CDCl_3$. Whenever appropriate, signal assignments were deduced from DEPT, COSY, and CH correlation NMR experiments. LC-MS was performed

DOI: 10.1021/acs.jmedchem.8b00095
J. Med. Chem. 2018, 61, 4087−4102

using an Agilent 1100 HPLC system over an Agilent Eclipse XDB-C8 column. Mass spectra were recorded on a Bruker Esquire ~ LC ion trap mass spectrometer (ESI). Column chromatography was performed using a LaFlash system (VWR) with Macherey-Nagel silica gel 60 (63−200 μm) for precolumns and prepacked Interchim PuriFlash-30SIHP silica gel columns (30 μm, 40 g) using mixtures of petroleum ether (PE) and ethyl acetate (EA). Where necessary, reactions were carried out in a nitrogen atmosphere using dry solvents. HPLC analysis was performed on a Hewlett-Packard 1050 Series using a ZORBAX Eclipse XDB-C8 column or an STAGROMA YMC-C-18 column. All test compounds were proved by HPLC to have ≥95% purity.

General Methods for the Synthesis of Isothiocyanate Precursors. *Method A. 1-(Bromomethyl)-benzene Derivatives.* To a solution of the appropriate benzyl alcohol in dichloromethane, phosphorus tribromide was added at 0 °C. The reaction mixture was allowed to warm to room temperature and stirred for an additional hour. The reaction was quenched with a saturated solution of sodium hydrogen carbonate and extracted with diethyl ether. The organic layer was washed with a saturated solution of sodium thiosulfate and brine, dried over sodium sulfate, and concentrated under vacuum. The obtained products were used without further purification.

1-(Isothiocyanatomethyl)-benzene Derivatives. 1-(Bromomethyl)-benzene derivatives were heated with potassium thiocyanate and sodium iodide in anhydrous dimethylformamide (DMF) at 90 °C for 7 h. The reaction mixture was poured into water and extracted with diethyl ether. The organic layer was washed three times with water, dried over sodium sulfate, and concentrated under vacuum. The crude product was purified by silica gel column flash chromatography (5% EA/PE).

Method B. 1-(Isothiocyanatomethyl)-benzene Derivatives. The appropriate amine dissolved in dichloromethane or tetrahydrofuran was stirred at 0 °C with trimethylamine for 10 min. Thiophosgene was added dropwise at 0 °C, and the mixture was stirred for additional 20 min, then allowed to reach room temperature and stirred for 3 h. The solution was acidified with aqueous HCl and extracted with dichloromethane. The combined organic phases were dried over sodium sulfate, and the solvent was removed under reduced pressure. The crude product was purified by silica gel column flash chromatography (5% EA/PE).

*1-(Bromomethyl)-4-(methoxy)benzene (**1**).* 1-(Bromomethyl)-4-(methoxy)benzene (**1**) was obtained from 4-methoxybenzyl alcohol (696 mg, 5.04 mmol) with phosphorus tribromide (352 μL, 3.75 mmol) in dichloromethane (20 mL) according to method A. Yield: 913 mg (90%); C_8H_9BrO (M_r 201.06); ^{1}H NMR ($CDCl_3$): δ = 7.25 (m_C, 2 H, C^2H_{ar}), 6.79 (m_C, 2 H, C^3H_{ar}), 4.43 (s, 2 H, CH_2), 3.74 (s, 3 H, CH_3) ppm; ^{13}C NMR ($CDCl_3$): δ = 159.7 (C^4_{ar}), 130.4 (C^2H_{ar}), 130.0 (C^1_{ar}), 114.2 (C^3H_{ar}), 55.3 (CH_3), 24.0 (CH_2) ppm; MS (ESI, 70 eV) m/z = not detected.

*1-(Isothiocyanatomethyl)-4-(methoxy)benzene (**2**).* 1-(Isothiocyanatomethyl)-4-(methoxy)benzene (**2**) was obtained from **1** (549 mg, 2.73 mmol) with potassium thiocyanate (480 mg, 4.94 mmol) and sodium iodide (60.0 mg, 0.40 mmol) in DMF (5 mL) according to method A. Yield: 325 mg (66%); C_9H_9NOS (M_r 179.24); ^{1}H NMR ($CDCl_3$): δ = 7.19−7.14 (m, 2 H, C^2H_{ar}), 6.84 (m_C, 2 H, C^3H_{ar}), 4.56 (s, 2 H, CH_2), 3.74 (s, 3 H, CH_3) ppm; ^{13}C NMR ($CDCl_3$): δ = 159.6 (C^4_{ar}), 131.9 (C^1_{ar}), 128.4 (C^2H_{ar}), 126.3 (N═C═S), 114.2 (C^3H_{ar}), 55.3 (CH_3), 48.3 (CH_2) ppm; MS (ESI, 70 eV) m/z = 356.9 $[MM]^+$.

*1-(Bromomethyl)-2,3-(dimethoxy)benzene (**3**).* 1-(Bromomethyl)-2,3-(dimethoxy)benzene (**3**) was obtained from 2,3-dimethoxybenzyl alcohol (842 mg, 5.01 mmol) with phosphorus tribromide (352 μL, 3.75 mmol) in dichloromethane (20 mL) according to method A. Yield: 845 mg (73%); $C_9H_{11}BrO_2$ (M_r 231.09); ^{1}H NMR ($CDCl_3$): δ = 7.04 (q, ^3J = 8.1 Hz, 1 H, C^6H_{ar}), 6.98 (dd, ^3J = 7.8 Hz, ^4J = 1.9 Hz, 1 H, C^5H_{ar}), 6.90 (dd, ^3J = 7.9 Hz, ^4J = 1.8 Hz, 1 H, C^4Har), 4.59 (s, 2 H, CH_2), 3.98 (s, 3 H, C^2O-CH_3), 3.89 (s, 3 H, C^3O-CH_3) ppm; ^{13}C NMR ($CDCl_3$): δ = 152.8 (C^2_{ar}), 147.4 (C^3_{ar}), 131.9 (C^1_{ar}), 124.2 (C^6H_{ar}), 122.5 (C^5H_{ar}), 113.0 (C^4H_{ar}), 60.8 (C^2O-CH_3), 55.8 (C^3O-CH_3), 28.1 (CH_2) ppm; MS (ESI, 70 eV) m/z = not detected.

*1-(Isothiocyanatomethyl)-2,3-(dimethoxy)benzene (**4**).* 1-(Isothiocyanatomethyl)-2,3-(dimethoxy)benzene (**4**) was obtained from **3** (586 mg, 2.53 mmol) with potassium thiocyanate (449 mg, 4.62 mmol) and sodium iodide (58.0 mg, 0.387 mmol) in DMF (4 mL) according to method A. Yield: 214 mg (41%); $C_{10}H_{11}NO_2S$ (M_r 209.26); ^{1}H NMR ($CDCl_3$): δ = 7.08 (t, ^3J = 7.9 Hz, 1 H, C^6H_{ar}), 6.93 (m_C, 2 H, C^4H_{ar}, C^5H_{ar}), 4.73 (s, 2 H, CH_2), 3.89 (s, 3 H, C^2O-CH_3), 3.88 (s, 3 H, C^3O-CH_3) ppm; ^{13}C NMR ($CDCl_3$): δ = 152.8 (C^2_{ar}), 146.6 (C^3_{ar}), 131.6 (N═C═S), 128.1 (C^1_{ar}), 124.4 (C^6H_{ar}), 120.4 (C^5H_{ar}), 113.0 (C^4H_{ar}), 61.1 (C^2O-CH_3), 56.0 (C^3O-CH_3), 44.1 (CH_2) ppm; MS (ESI, 70 eV) m/z = 417.0 $[MM]^+$.

*1-(Isothiocyanatomethyl)-3-(trifluoromethyl)benzene (**5**).* 1-(Isothiocyanatomethyl)-3-trifluoromethylbenzene (**5**) was obtained from 3-trifluoro-methyl benzylamine (220 μL, 1.53 mmol) with thiophosgene (120 μL, 1.57 mmol) and trimethylamine (840 μL, 6.06 mmol) in dichloromethane (10 mL) according to method B. Yield: 90.0 mg (28%); $C_9H_6F_3NS$ (M_r 217.21); ^{1}H NMR ($CDCl_3$): δ = 7.63−7.53 (m, 1 H, C^2H_{ar}), 7.57−7.53 (m, 3 H, C^4H_{ar}, C^5H_{ar}, C^6H_{ar}), 4.80 (s, 2 H, CH_2) ppm; ^{13}C NMR ($CDCl_3$): δ = 135.3 (C^1_{ar}), 133.9 (N═C═S), 131.4 (d, $^2J_{CF}$ = 32.7 Hz, C^3_{ar}), 130.1 (d, $^4J_{CF}$ = 1.7 Hz. C^5H_{ar}), 129.6 (C^6H_{ar}), 125.3 (q, $^3J_{CF}$ = 3.8 Hz, C^2H_{ar}), 123.8 (d, $^1J_{CF}$ = 272.5 Hz, CF_3), 123.7 (q, $^3J_{CF}$ = 3.8 Hz, C^4H_{ar}), 48.3 (CH_2) ppm; MS (ESI, 70 eV) m/z = 432.9 $[MM]^+$.

*1-(Isothiocyanatomethyl)-4-(trifluoromethyl)benzene (**6**).* 1-(Isothiocyanatomethyl)-4-trifluoromethylbenzene (**6**) was obtained from 4-trifluoro-methyl benzylamine (715 μL, 5.02 mmol) with thiophosgene (410 μL, 5.35 mmol) and trimethylamine (2.80 mL, 20.2 mmol) in dichloromethane (27 mL) according to method B. Yield: 625 mg (56%); $C_9H_6F_3NS$ (M_r 217.21); ^{1}H NMR ($CDCl_3$): δ = 7.68 (d, ^3J = 8.0 Hz, 2 H, C^3H_{ar}), 7.47 (dt, ^3J = 8.0 Hz, ^4J = 0.7 Hz, 2 H, C^2H_{ar}), 4.82 (s, 2 H, CH_2) ppm; ^{13}C NMR ($CDCl_3$): δ = 138.2 (C^1_{ar}), 130.7 (d, $^2J_{CF}$ = 32.8 Hz, C^4_{ar}), 129.9 (N═C═S), 127.1 (C^2H_{ar}), 125.0 (q, $^3J_{CF}$ = 3.8 Hz, C^3H_{ar}), 123.8 (d, $^1J_{CF}$ = 271.8 Hz, CF_3), 48.2 (CH_2) ppm; MS (ESI, 70 eV) m/z = not detected.

*1-(Isothiocyanatomethyl)-4-(trifluoromethoxy)benzene (**7**).* 1-(Isothiocyanatomethyl)-4-(trifluoromethoxy)benzene (**7**) was obtained from 4-trifluoro-methoxy benzylamine (382 μL, 2.50 mmol) with thiophosgene (200 μL, 2.61 mmol) and trimethylamine (1.39 mL, 10.0 mmol) in tetrahydrofuran (13 mL) according to method B. Yield: 360 mg (62%); $C_9H_6F_3NOS$ (M_r 233.21); ^{1}H NMR ($CDCl_3$): δ = 7.40−7.36 (m, 2 H, C^2H_{ar}), 7.27 (d, ^3J = 8.4 Hz, 2 H, C^3H_{ar}), 4.75 (s, 2 H, CH_2) ppm; ^{13}C NMR ($CDCl_3$): δ = 149.1 (d, $^3J_{CF}$ = 1.8 Hz, C^4_{ar}), 133.0 (C^2H_{ar}), 128.4 (C^1_{ar}), 125.5 (N═C═S), 120.4 (d, $^1J_{CF}$ = 257.7 Hz, CF_3), 121.5 (C^3H_{ar}), 48.2 (CH_2) ppm; MS (ESI, 70 eV) m/z = 464.9 $[MM]^+$.

*Methyl 3-Amino-4,5-dihydrothiophene-2-carboxylate (**8**).* To a solution of 1,8-diazabicyclo[5.4.0]undec-7-ene (DBU, 10.0 mL, 67.0 mmol) in anhydrous methanol (25 mL) under nitrogen atmosphere was added methyl thioglycolate (4.20 mL, 46.7 mmol) at 0 °C. Acrylonitrile (3.30 mL, 49.8 mmol) was added dropwise, and the solution was stirred at 0 °C for 5 h and at 80 °C overnight. After cooling to room temperature, the solvent was evaporated and quenched with a saturated solution of ammonium chloride. The aqueous phase was extracted with ethyl acetate (3 × 100 mL), the organic layer was dried over sodium sulfate, and the solvent was removed under reduced pressure. The crude product was purified by silica gel column chromatography (30% EA/PE) to obtain (**8**) as yellow solid. Yield: 3.20 g (43%); $C_6H_9NO_2S$ (M_r 159.21); ^{1}H NMR (DMSO-d_6): δ = 7.08 (s, 2 H, NH_2), 3.57 (s, 3 H, CH_3), 2.96−2.91 (m, 2 H, SCH_2CH_2), 2.85−2.78 (m, 2 H, SCH_2CH_2) ppm; ^{13}C NMR (DMSO-d_6): δ = 165.1 (C═O), 159.2 (C_q-NH_2), 85.9 (SC_qC═O), 50.3 (CH_3), 38.4 (SCH_2CH_2), 26.9 (SCH_2CH_2) ppm; MS (ESI, 70 eV) m/z = 316.9 $[MM]^+$, 159.8 $[M + H]^+$.

General Method for the Synthesis of Tetrahydrothienopyrimidinone Derivatives. The appropriate isothiocyanate was heated with methyl 3-amino-4,5-dihydrothiophene-2-carboxylate in anhydrous pyridine at 110 °C under nitrogen atmosphere for 24 h. After cooling of the solution, the solvent was evaporated and the residue was purified by silica gel column flash chromatography (gradient EE/PE).

DOI: 10.1021/acs.jmedchem.8b00095
J. Med. Chem. 2018, 61, 4087−4102

*3-Phenyl-2-thioxo-2,3,6,7-tetrahydrothieno[3,2-d]pyrimidin-4(1H)-one (**9**).* 3-Phenyl-2-thioxo-2,3,6,7-tetrahydrothieno[3,2-*d*]-pyrimidin-4(1*H*)-one (**9**) was obtained from commercially available phenyl isothiocyanate (420 μL, 3.51 mmol) with **8** (461 mg, 2.90 mmol) in anhydrous pyridine (9 mL). After silica gel column flash chromatography (gradient EE/PE starting with 30% EE), the obtained product was washed three times with ethyl acetate. Yield: 113 mg (15%); $C_{12}H_{10}N_2OS_2$ (M_r 262.35); ^{1}H NMR ($CDCl_3$): δ = 13.23 (s, 1 H, N*H*), 7.49−7.35 (m, 3 H, C^2*H*$_{phen}$, C^4*H*$_{phen}$), 7.19−7.16 (m, 2 H, C^3*H*$_{phen}$), 3.41−3.36 (m, 2 H, SCH$_2$C*H*$_2$), 3.28−3.22 (m, 2 H, SC*H*$_2$CH$_2$) ppm; ^{13}C NMR ($CDCl_3$): δ = 175.3 (*C*═S), 156.9 (C═O), 149.5 (*C*$_q$NHR), 139.1 (*C*^{1}*H*$_{phen}$), 129.0 (*C*^{3}*H*$_{phen}$), 128.6 (*C*^{2}*H*$_{phen}$), 128.2 (*C*^{4}*H*$_{phen}$), 114.4 (*SC*$_q$C═O), 34.6 (*SCH*$_2$CH$_2$), 29.0 (SCH$_2$*CH*$_2$) ppm; MS (ESI, 70 eV) *m*/*z* = 262.8 [MM]$^+$.

*3-Benzyl-2-thioxo-2,3,6,7-tetrahydrothieno[3,2-d]pyrimidine-4(1H)-one (**10**).* 3-Benzyl-2-thioxo-2,3,6,7-tetrahydrothieno[3,2-*d*]-pyrimidine-4(1*H*)-one (**10**) was obtained from commercially available benzyl isothiocyanate (560 μL, 4.22 mmol) with **8** (596 mg, 3.74 mmol) in anhydrous pyridine (12 mL).

After silica gel column flash chromatography (gradient EE/PE starting with 30% EE), the obtained product was washed three times with ethyl acetate. Yield: 207 mg (20%); $C_{13}H_{12}N_2OS_2$ (M_r 276.38); ^{1}H NMR (DMSO-d_6): δ = 13.24 (s, 1 H, N*H*), 7.30−7.21 (m, 5 H, C^2*H*$_{benz}$, C^3*H*$_{benz}$, C^4*H*$_{benz}$), 5.53 (s, 2 H, N-C*H*$_2$), 3.38−3.32 (m, 2 H, SCH$_2$C*H*$_2$), 3.24−3.18 (m, 2 H, SC*H*$_2$CH$_2$) ppm; ^{13}C NMR (DMSO-d_6): δ = 174.5 (*C*═S), 156.6 (C═O), 149.3 (*C*$_q$NHR), 136.2 (*C*^{1}*H*$_{benz}$), 128.2 (*C*^{3}*H*$_{benz}$), 127.2 (*C*^{2}*H*$_{benz}$), 127.0 (*C*^{4}*H*$_{benz}$), 114.0 (*SC*$_q$C═O), 48.7 (N-*C*H$_2$), 34.5 (*SCH*$_2$CH$_2$), 28.9 (SCH$_2$*CH*$_2$) ppm; MS (ESI, 70 eV) *m*/*z* = 276.7 [M + H]$^+$.

*3-(4-Methoxybenzyl)-2-thioxo-2,3,6,7-tetrahydrothieno[3,2-d]-pyrimidin-4(1H)-one (**11**).* 3-(4-Methoxybenzyl)-2-thioxo-2,3,6,7-tetrahydrothieno[3,2-*d*]pyrimidin-4(1*H*)-one (**11**) was obtained from **2** (313 mg, 1.75 mmol) with **8** (269 mg, 1.69 mmol) in anhydrous pyridine (5 mL). The crude product was purified by silica gel column flash chromatography (gradient EE/PE starting with 20% EE). Yield: 120 mg (23%); $C_{14}H_{14}N_2O_2S_2$ (M_r 306.40); ^{1}H NMR (DMSO-d_6): δ = 13.19 (s, 1 H, N*H*), 7.29 (d, ^3J = 8.8 Hz, 2 H, C^2*H*$_{benz}$), 6.85 (d, ^3J = 8.8 Hz, 2 H, C^3*H*$_{benz}$), 5.45 (s, 2 H, N-C*H*$_2$), 3.71 (s, 3 H, CH$_3$), 3.33 (t, ^3J = 8.0 Hz, 2 H, SCH$_2$C*H*$_2$), 3.20 (t, ^3J = 8.0 Hz, 2 H, SC*H*$_2$CH$_2$) ppm; ^{13}C NMR (DMSO-d_6): δ = 174.4 (*C*═S), 158.4 (C═O), 156.6 (C^4*H*$_{benz}$), 149.2 (*C*$_q$NHR), 129.1 (C^2*H*$_{benz}$), 128.2 (*C*^{1}*H*$_{benz}$), 114.1 (*SC*$_q$C═O), 113.5 (C^3*H*$_{benz}$), 55.0 (CH$_3$), 48.1 (N-*C*H$_2$), 34.5 (*SCH*$_2$CH$_2$), 28.9 (SCH$_2$*CH*$_2$) ppm; MS (ESI, 70 eV) *m*/*z* = 306.9 [M + H]$^+$.

*3-(2,3-Dimethoxybenzyl)-2-thioxo-2,3,6,7-tetrahydrothieno[3,2-d]pyrimidin-4(1H)-one (**12**).* 3-(2,3-Dimethoxybenzyl)-2-thioxo-2,3,6,7-tetrahydrothieno[3,2-*d*]pyrimidin-4(1*H*)-one (**12**) was obtained from **4** (495 mg, 1.75 mmol) with **8** (432 mg, 2.71 mmol) in anhydrous pyridine (8 mL). After silica gel column flash chromatography (gradient EE/PE starting with 20% EE), the obtained product was washed three times with ethyl acetate. Yield: 226 mg (28%); $C_{15}H_{16}N_2O_3S_2$ (M_r 336.43); ^{1}H NMR (DMSO-d_6): δ = 13.25 (s, 1 H, N*H*), 6.92 (m, 2 H, C^4*H*$_{benz}$, C^5*H*$_{benz}$), 6.35−6.32 (m, 1 H, C^6*H*$_{benz}$), 5.52 (s, 2 H, N-C*H*$_2$), 3.80 (s, 6 H, CH$_3$), 3.36 (t, ^3J = 8.0 Hz, 2 H, SCH$_2$C*H*$_2$), 3.24 (t, ^3J = 7.7 Hz, 2 H, SC*H*$_2$CH$_2$) ppm; ^{13}C NMR (DMSO-d_6): δ = 174.6 (*C*═S), 156.5 (C═O), 152.3 (C^2*H*$_{benz}$), 149.3 (*C*$_q$NHR), 145.8 (C^3*H*$_{benz}$), 129.3 (*C*^{1}*H*$_{benz}$), 123.7 (C^5*H*$_{benz}$), 117.0 (C^6*H*$_{benz}$), 113.8 (*SC*$_q$C═O), 111.5 (C^4*H*$_{benz}$), 59.6 (C^2*H*$_{benz}$-OCH$_3$), 55.6 (C^3*H*$_{benz}$-OCH$_3$), 44.5 (N-*C*H$_2$), 34.5 (*SCH*$_2$CH$_2$), 28.9 (SCH$_2$*CH*$_2$) ppm; MS (ESI, 70 eV) *m*/*z* = 336.9 [M + H]$^+$.

*2-Thioxo-3-(3-(trifluoromethyl)benzyl)-2,3,6,7-tetrahydrothieno-[3,2-d]pyrimidin-4(1H)-one (**13**).* 2-Thioxo-3-(3-(trifluoromethyl)-benzyl)-2,3,6,7-tetrahydrothieno[3,2-*d*]pyrimidin-4(1*H*)-one (**13**) was obtained from **5** (598 mg, 2.75 mmol) with **8** (366 mg, 2.30 mmol) in anhydrous pyridine (7 mL). After evaporating the solvent, the residue was washed with dichloromethane, and the product was obtained as beige solid. Yield: 250 mg (32%); $C_{14}H_{11}F_3N_2OS_2$ (M_r 344.38); ^{1}H NMR (DMSO-d_6): δ = 13.30 (s, 1 H, N*H*), 7.70 (bs, 1 H, C^2*H*$_{benz}$), 7.63−7.52 (m, 3 H, C^4*H*$_{benz}$, C^5*H*$_{benz}$, C^6*H*$_{benz}$), 5.60 (s, 2 H, N-C*H*$_2$), 3.35 (t, ^3J = 8.0 Hz, 2 H, SCH$_2$C*H*$_2$), 3.22 (t, ^3J = 7.9 Hz, 2 H, SC*H*$_2$CH$_2$) ppm; ^{13}C NMR (DMSO-d_6): δ = 174.4 (*C*═S), 156.7 (C═O), 149.6 (*C*$_q$NHR), 137.7 (C^1*H*$_{benz}$), 131.3 (*C*^{6}*H*$_{benz}$), 129.3 (*C*^{5}*H*$_{benz}$), 128.9 (d, $^2J_{CF}$ = 31.4 Hz, C^3*H*$_{benz}$), 124.1 (d, $^1J_{CF}$ = 272.3 Hz, *C*F$_3$), 124.1 (d, $^3J_{CF}$ = 3.8 Hz, *C*^{2}H$_{benz}$), 123.9 (d, $^3J_{CF}$ = 3.7 Hz, *C*^{4}H$_{benz}$), 114.0 (*SC*$_q$C═O), 48.5 (N-*C*H$_2$), 34.5 (*SCH*$_2$CH$_2$), 28.9 (SCH$_2$*CH*$_2$) ppm; MS (ESI, 70 eV) *m*/*z* = 344.9 [M + H]$^+$.

*2-Thioxo-3-(4-(trifluoromethyl)benzyl)-2,3,6,7-tetrahydrothieno-[3,2-d]pyrimidin-4(1H)-one (**14**).* 2-Thioxo-3-(4-(trifluoromethyl)-benzyl)-2,3,6,7-tetrahydrothieno[3,2-*d*]pyrimidin-4(1*H*)-one (**14**) was obtained from **6** (550 mg, 2.53 mmol) with **8** (358 mg, 2.25 mmol) in anhydrous pyridine (7 mL). After evaporating the solvent, the residue was washed with dichloromethane, and the product was obtained as beige solid. Yield: 373 mg (48%); $C_{14}H_{11}F_3N_2OS_2$ (M_r 344.38); ^{1}H NMR (DMSO-d_6): δ = 13.32 (s, 1 H, N*H*), 7.67 (d, ^3J = 8.2 Hz, 2 H, C^3*H*$_{benz}$), 7.47 (d, ^3J = 8.2 Hz, 2 H, C^2*H*$_{benz}$), 5.60 (s, 2 H, N-C*H*$_2$), 3.39−3.33 (m, 2 H, SCH$_2$C*H*$_2$), 3.26−3.20 (m, 2 H, SC*H*$_2$CH$_2$) ppm; ^{13}C NMR (DMSO-d_6): δ = 174.5 (*C*═S), 156.6 (C═O), 149.6 (*C*$_q$NHR), 141.1 (C^1*H*$_{benz}$), 127.6 (*C*^{2}*H*$_{benz}$), 127.6 (d, $^2J_{CF}$ = 32.2 Hz, *C*^{4}H$_{benz}$), 125.1 (q, $^3J_{CF}$ = 3.9 Hz, *C*^{3}H$_{benz}$), 124.3 (d, $^1J_{CF}$ = 271.8 Hz, *C*F$_3$), 114.0 (*SC*$_q$C═O), 48.6 (N-*C*H$_2$), 34.5 (*SCH*$_2$CH$_2$), 29.0 (SCH$_2$*CH*$_2$) ppm; MS (ESI, 70 eV) *m*/*z* = 344.9 [M + H]$^+$.

*2-Thioxo-3-(4-(trifluoromethoxy)benzyl)-2,3,6,7-tetrahydrothieno[3,2-d]pyrimidin-4(1H)-one (**15**).* 2-Thioxo-3-(4-(trifluoromethoxy)benzyl)-2,3,6,7-tetrahydrothieno[3,2-*d*]pyrimidin-4(1*H*)-one (**15**) was obtained from **7** (294 mg, 1.26 mmol) with **8** (181 mg, 1.14 mmol) in anhydrous pyridine (3.5 mL). After silica gel column flash chromatography (gradient EE/PE starting with 10% EE) the obtained product was obtained as beige solid. Yield: 112 mg (27%); $C_{14}H_{11}F_3N_2O_2S_2$ (M_r 360.37); ^{1}H NMR (DMSO-d_6): δ = 13.28 (s, 1 H, N*H*), 7.43 (d, ^3J = 8.4 Hz, 2 H, C^3*H*$_{benz}$), 7.30 (d, ^3J = 8.3 Hz, 2 H, C^2*H*$_{benz}$), 5.54 (s, 2 H, N-C*H*$_2$), 3.34 (t, ^3J = 7.5 Hz, 2 H, SCH$_2$C*H*$_2$), 3.22 (t, ^3J = 7.7 Hz, 2 H, SC*H*$_2$CH$_2$) ppm; ^{13}C NMR (DMSO-d_6): δ = 174.4 (*C*═S), 156.6 (C═O), 149.5 (*C*$_q$NHR), 147.3 (C^4*H*$_{benz}$), 135.7 (C^1*H*$_{benz}$), 129.2 (C^2*H*$_{benz}$), 120.8 (C^3*H*$_{benz}$), 120.1 (d, $^1J_{CF}$ = 255.9 Hz, *C*F$_3$), 114.1 (*SC*$_q$C═O), 48.2 (N-*C*H$_2$), 34.5 (*SCH*$_2$CH$_2$), 29.0 (SCH$_2$*CH*$_2$) ppm; MS (ESI, 70 eV) *m*/*z* = 360.9 [M + H]$^+$.

*2-Chloro-N-(6-(trifluoromethyl)benzo[d]thiazol-2-yl)acetamide (**16**).* A mixture of 5-(trifluoromethyl)benzo[*d*]thiazol-2-amine (596 mg, 2.73 mmol) and trimethylamine (453 μL, 3.27 mmol) in dichloromethane (6 mL) was added over a period of 10 min to a solution of 2-chloracetyl chloride (239 μL, 3.00 mmol) in dichloromethane (4 mL). The reaction mixture was kept under stirring for 24 h and then concentrated in vacuum. The obtained product was washed with water and dried in vacuum. Yield: 596 g (74%); $C_{10}H_6ClF_3N_2OS$ (M_r 294,68); ^{1}H NMR (DMSO-d_6): δ = 12.96 (s, 1 H, N*H*), 8.52 (d, ^4J = 1.6 Hz, 1 H, C^7*H*$_{benzth}$), 7.94 (d, ^3J = 8.5 Hz, 1 H, C^4*H*$_{benzth}$), 7.75 (dd, ^3J = 8.5 Hz, ^4J = 1.6 Hz, 1 H, C^5*H*$_{benzth}$), 4.50 (s, 2 H, *C*H$_2$-Cl) ppm; ^{13}C NMR (DMSO-d_6): δ = 166.4 (*C*═O), 160.8 (C^2$_{benzth}$), 151.2 (C^{3a}$_{benzth}$), 132.0 (C^{7a}$_{benzth}$), 124.5 (d, $^1J_{CF}$ = 271.8 Hz, *C*F$_3$), 123.9 (d, $^2J_{CF}$ = 31.9 Hz, C^6$_{benzth}$), 123.0 (d, $^3J_{CF}$ = 3.6 Hz, C^{5}H$_{benzth}$), 121.2 (C^{4}H$_{benzth}$), 120.0 (d, $^3J_{CF}$ = 4.0 Hz, C^{7}H$_{benzth}$), 42.5 (CH$_2$-Cl) ppm; MS (ESI, 70 eV) *m*/*z* = 294.8 [M + H]$^+$.

General Method for the Synthesis of IWP-Derived Compounds. Appropriate acetamide and tetrahydrothieno-pyrimidinone derivative was dissolved in DMF under a positive pressure of nitrogen. Triethylamine was added, and the mixture was stirred at 80 °C for 2 h. The reaction mixture was cooled to room temperature and quenched with water. The organic layer was separated, and the aqueous layer was extracted with ethyl ether (3 times). The combined organic phases were washed three times each with water and brine, dried over sodium sulfate, and the solvent was reduced in vacuum. The crude product was purified by silica gel column flash chromatography (gradient EE/PE).

*2-((4-Oxo-3-phenyl-3,4,6,7-tetrahydrothieno[3,2-d]pyrimidin-2-yl)thio)-N-(6-(trifluoromethyl)benzo[d]thiazol-2-yl)acetamide (**17**).* 2-((4-Oxo-3-phenyl-3,4,6,7-tetrahydrothieno[3,2-*d*]pyrimidin-2-yl)-thio)-*N*-(6-(trifluoromethyl)benzo[*d*]thiazol-2-yl)acetamide (**17**) was obtained from **16** (220 mg, 0.747 mmol), **9** (186 mg, 0.708 mmol) and triethylamine (300 μL, 2.16 mmol) in DMF (7 mL). The crude

DOI: 10.1021/acs.jmedchem.8b00095
J. Med. Chem. 2018, 61, 4087−4102

product was purified by silica gel column chromatography (gradient EE/PE starting with 20% EE). Yield: 95 mg (26%); $C_{22}H_{15}F_3N_4O_2S_3$ (M_r 520.57); HPLC (purity): 97%; ^{1}H NMR (DMSO-d_6): δ = 12.85 (s, 1 H, N*H*), 8.50 (dd, ^4J = 1.6 Hz, ^5J = 0.6 Hz, 1 H, C^7*H*$_{benzth}$), 7.92 (d, ^3J = 8.5 Hz, 1 H, C^4*H*$_{benzth}$), 7.76−7.73 (m, 1 H, C^5*H*$_{benzth}$), 7.62−7.57 (m, 3 H, C^{3}H$_{phen}$, C^{4}H$_{phen}$), 7.46−7.42 (m, 2 H, C^{2}H$_{phen}$), 4.16 (s, 2 H, C*H*$_2$-C=O), 3.30 (t, ^3J = 8.1 Hz, 2 H, SCH$_2$C*H*$_2$), 3.10 (t, ^3J = 8.1 Hz, 2 H, SC*H*$_2$CH$_2$) ppm; ^{13}C NMR (DMSO-d_6): δ = 167.6 (CH$_2$−*C*=O), 161.0 (C$^2_{benzth}$), 160.5 (*C*$_q$N=C−S), 158.5 (N=*C*$_q$-S), 156.9 (NRR'-*C*=O), 151.3 (C$^{3a}_{benzth}$), 135.4 (*C*$^1_{phen}$), 132.0 (*C*$^{7a}_{benzth}$), 130.2 (*C*^{3}H$_{phen}$), 129.7 (*C*^{4}H$_{phen}$), 128.8 (*C*^{2}H$_{phen}$), 124.5 (d, $^1J_{CF}$ = 271.7 Hz, *C*F$_3$), 123.8 (d, $^2J_{CF}$ = 31.5 Hz, C$^6_{benzth}$), 122.9 (d, $^3J_{CF}$ = 3.2 Hz, *C*^{5}H$_{benzth}$), 121.0 (*C*^{4}H$_{benzth}$), 119.9 (SC$_q$C=O), 119.8 (*C*^{7}H$_{benzth}$), 37.1 (SCH$_2$CH$_2$), 36.1 (CH$_2$−C=O), 28.4 (SCH$_2$*C*H$_2$) ppm; MS (ESI, 70 eV) m/z = 520.8 [M + H]$^+$; IR: 3173, 3073, 1707, 1647, 1545, 1308, 1244, 1121, 756, 698 cm^{-1}.

*2-((3-Benzyl-4-oxo-3,4,6,7-tetrahydrothieno[3,2-d]pyrimidin-2-yl)thio)-N-(6-(trifluoromethyl)benzo[d]thiazol-2-yl)acetamide (**18**).* 2-((3-Benzyl-4-oxo-3,4,6,7-tetrahydrothieno[3,2-*d*]pyrimidin-2-yl)-thio)-*N*-(6-(trifluoromethyl)benzo[*d*]thiazol-2-yl)acetamide (**18**) was obtained from **16** (235 mg, 0.797 mmol), **10** (196 mg, 0.709 mmol) and triethylamine (300 μL, 2.16 mmol) in DMF (7 mL). The crude product was purified by silica gel column flash chromatography (gradient EE/PE starting with 20% EE). Yield: 278 mg (73%); $C_{23}H_{17}F_3N_4O_2S_3$ (M_r 534.60); HPLC (purity): 100%; ^{1}H NMR (DMSO-d_6): δ = 12.92 (s, 1 H, N*H*), 8.49 (dd, ^4J = 1.3 Hz, ^5J = 0.6 Hz, 1 H, C^7*H*$_{benzth}$), 7.92 (d, ^3J = 8.5 Hz, 1 H, C^4*H*$_{benzth}$), 7.74 (dd, ^3J = 8.6 Hz, ^4J = 1.5 Hz, 1 H, C^5*H*$_{benzth}$), 7.40−7.25 (m, 5 H, C^2*H*$_{phen}$, C^3*H*$_{phen}$, C^4*H*$_{phen}$), 5.27 (s, 2 H, N-C*H*$_2$), 4.27 (s, 2 H, C*H*$_2$-C=O), 3.27 (t, ^3J = 8.5 Hz, 2 H, SCH$_2$C*H*$_2$), 3.04 (t, ^3J = 8.5 Hz, 2 H, SC*H*$_2$CH$_2$) ppm; ^{13}C NMR (DMSO-d_6): δ = 167.5 (CH$_2$−*C*=O), 161.0 (C$^2_{benzth}$), 160.4 (*C*$_q$N=C−S), 158.0 (N=*C*$_q$-S), 157.1 (NRR'-C=O), 151.3 (C$^{3a}_{benzth}$), 134.9 (*C*$^1_{benz}$), 132.0 (*C*$^{7a}_{benzth}$), 128.6 (*C*^{3}H$_{benz}$), 127.7 (*C*^{4}H$_{benz}$), 127.0 (*C*^{2}H$_{phen}$), 124.5 (d, $^1J_{CF}$ = 271.9 Hz, *C*F$_3$), 123.8 (d, $^2J_{CF}$ = 31.8 Hz, C$^6_{benzth}$), 123.0 (d, $^3J_{CF}$ = 3.8 Hz, *C*^{5}H$_{benzth}$), 121.0 (*C*^{4}H$_{benzth}$), 119.9 (d, $^3J_{CF}$ = 4.3 Hz, *C*^{7}H$_{benzth}$), 119.4 (SC$_q$C=O), 47.1 (N-CH$_2$) 36.9 (SCH$_2$CH$_2$), 36.0 (CH$_2$−C=O), 28.4 (SCH$_2$CH$_2$) ppm; MS (ESI, 70 eV) m/z = 534.9 [M + H]$^+$; IR: 3821, 3769, 2320, 1688, 1545, 1474, 1317, 1105, 835, 735, 696 cm^{-1}.

*2-((3-(4-Methoxybenzyl)-4-oxo-3,4,6,7-tetrahydrothieno[3,2-d]pyrimidin-2-yl)thio)-N-(6-(trifluoromethyl)benzo[d]thiazol-2-yl)acetamide (**19**).* 2-((3-(4-Methoxybenzyl)-4-oxo-3,4,6,7-tetrahydrothieno[3,2-*d*]pyrimidin-2-yl)thio)-*N*-(6-(trifluoromethyl)-benzo[*d*]thiazol-2-yl)acetamide (**19**) was obtained from **16** (98.0 mg, 0.335 mmol), **11** (98.6 mg, 0.320 mmol), and triethylamine (132 μL, 0.952 mmol) in DMF (4 mL). The crude product was purified by silica gel column flash chromatography (gradient EE/PE starting with 20% EE). Yield: 126 mg (69%); $C_{24}H_{19}F_3N_4O_3S_3$ (M_r 564.62); HPLC (purity): 98%; ^{1}H NMR (DMSO-d_6): δ = 12.91 (s, 1 H, N*H*), 8.49 (dd, ^4J = 1.2 Hz, ^5J = 0.7 Hz, 1 H, C^7*H*$_{benzth}$), 7.92 (d, ^3J = 8.5 Hz, 1 H, C^4*H*$_{benzth}$), 7.75 (dd, ^3J = 8.5 Hz, ^4J = 1.4 Hz, 1 H, C^5*H*$_{benzth}$), 7.24 (d, ^3J = 8.8 Hz, 2 H, C^2*H*$_{benz}$), 6.92 (d, ^3J = 8.8 Hz, 2 H, C^3*H*$_{benz}$), 5.19 (s, 2 H, N-C*H*$_2$), 4.26 (s, 2 H, C*H*$_2$-C=O), 3.74 (s, 3 H, C*H*$_3$), 3.26 (t, ^3J = 8.6 Hz, 2 H, SCH$_2$C*H*$_2$), 3.02 (t, ^3J = 8.6 Hz, 2 H, SC*H*$_2$CH$_2$) ppm; ^{13}C NMR (DMSO-d_6): δ = 167.5 (CH$_2$−*C*=O), 161.0 (C$^2_{benzth}$), 160.3 (*C*$_q$N=C−S), 158.8 (*C*$^4_{benz}$), 157.9 (N=*C*$_q$-S), 157.0 (NRR'-*C*=O), 151.3 (C$^{3a}_{benzth}$), 132.0 (*C*$^{7a}_{benzth}$), 128.7 (*C*^{2}H$_{benz}$), 126.8 (*C*$^1_{benz}$), 124.5 (d, $^1J_{CF}$ = 273.1 Hz, *C*F$_3$), 123.8 (d, $^2J_{CF}$ = 31.9 Hz, C$^6_{benzth}$), 123.0 (d, $^3J_{CF}$ = 3.4 Hz, *C*^{5}H$_{benzth}$), 121.0 (*C*^{4}H$_{benzth}$), 119.9 (d, $^3J_{CF}$ = 4.1 Hz, *C*^{7}H$_{benzth}$), 119.4 (SC$_q$C=O), 114.0 (*C*^{3}H$_{benz}$), 55.1 (CH$_3$), 46.6 (N-CH$_2$), 36.9 (SCH$_2$CH$_2$), 35.9 (CH$_2$−C=O), 28.4 (SCH$_2$CH$_2$) ppm; MS (ESI, 70 eV) m/z = 565.0 [M + H]$^+$; IR: 2875, 1707, 1686, 1528, 1472, 1325, 1273, 1105, 828, 650 cm^{-1}.

*2-((3-(2,3-Dimethoxybenzyl)-4-oxo-3,4,6,7-tetrahydrothieno[3,2-d]pyrimidin-2-yl)thio)-N-(6-(trifluoromethyl)benzo[d]thiazol-2-yl)acetamide (**20**).* 2-((3-(2,3-Dimethoxybenzyl)-4-oxo-3,4,6,7-tetrahydrothieno[3,2-*d*]pyrimidin-2-yl)thio)-*N*-(6-(trifluoromethyl)-benzo[*d*]thiazol-2-yl)acetamide (**20**) was obtained from **16** (216 mg, 0.733 mmol), **12** (240 mg, 0.713 mmol) and triethylamine (290 μL, 2.09 mmol) in DMF (7 mL). The crude product was purified by silica gel column flash chromatography (gradient EE/PE starting with 20% EE). Yield: 378 mg (89%); $C_{25}H_{21}F_3N_4O_4S_3$ (M_r 594.65); HPLC (purity): 100%; ^{1}H NMR (DMSO-d_6): δ = 12.89 (s, 1 H, N*H*), 8.49 (dd, ^4J = 1.2 Hz, ^5J = 0.7 Hz, 1 H, C^7*H*$_{benzth}$), 7.92 (d, ^3J = 8.5 Hz, 1 H, C^4*H*$_{benzth}$), 7.75 (dd, ^3J = 8.5 Hz, ^4J = 1.9 Hz, 1 H, C^5*H*$_{benzth}$), 7.05−6.99 (m, 2 H, C^4*H*$_{benz}$, C^5*H*$_{benz}$), 6.34 (dd, ^3J = 5.9 Hz, ^4J = 3.4 Hz, 1 H, C^6*H*$_{benz}$), 5.27 (s, 2 H, N-C*H*$_2$), 4.25 (s, 2 H, C*H*$_2$-C=O), 3.84 (s, 3 H, C$^2_{benz}$-OC*H*$_3$), 3.83 (C$^3_{benz}$-OC*H*$_3$), 3.28 (t, ^3J = 8.7 Hz, 2 H, SCH$_2$C*H*$_2$), 3.06 (t, ^3J = 8.7 Hz, 2 H, SC*H*$_2$CH$_2$) ppm; ^{13}C NMR (DMSO-d_6): δ = 167.4 (CH$_2$−*C*=O), 161.0 (C$^2_{benzth}$), 160.4 (*C*$_q$N=C−S), 158.1 (N=*C*$_q$-S), 157.0 (NRR'-*C*=O), 152.3 (*C*$^2_{benz}$), 151.3 (C$^{3a}_{benzth}$), 146.0 (*C*$^3_{benz}$), 132.9 (*C*$^{7a}_{benzth}$), 127.9 (*C*$^1_{benz}$), 124.5 (d, $^1J_{CF}$ = 271.4 Hz, *C*F$_3$), 124.2 (*C*^{5}H$_{benz}$), 123.8 (d, $^2J_{CF}$ = 32.0 Hz, C$^6_{benzth}$), 122.9 (d, $^3J_{CF}$ = 3.3 Hz, *C*^{5}H$_{benzth}$), 121.0 (*C*^{4}H$_{benzth}$), 119.9 (d, $^3J_{CF}$ = 3.2 Hz, *C*^{7}H$_{benzth}$), 119.2 (SC$_q$C=O), 117.2 (*C*^{6}H$_{benz}$), 112.2 (*C*^{4}H$_{benz}$), 60.0 (C$^2_{benz}$-OCH$_3$), 55.7 (C$^3_{benz}$-OCH$_3$), 42.4 (N-*C*H$_2$), 36.9 (SCH$_2$CH$_2$), 35.9 (CH$_2$-C=O), 28.4 (SCH$_2$*C*H$_2$) ppm; MS (ESI, 70 eV) m/z = 595.0 [M + H]$^+$; IR: 2940, 2839, 1672, 1541, 1476, 1317, 1273, 1130, 1080, 822, 745, 669 cm^{-1}.

*2-((4-Oxo-3-(3-(trifluoromethyl)benzyl)-3,4,6,7-tetrahydrothieno-[3,2-d]pyrimidin-2-yl)thio)-N-(6-(trifluoromethyl)benzo[d]thiazol-2-yl)acetamide (**21**).* 2-((4-Oxo-3-(3-(trifluoromethyl)benzyl)-3,4,6,7-tetrahydrothieno[3,2-*d*]pyrimidin-2-yl)thio)-*N*-(6-(trifluoromethyl)-benzo[*d*]thiazol-2-yl)acetamide (**21**) was obtained from **16** (86.6 mg, 0.294 mmol), **13** (103 mg, 0.299 mmol) and triethylamine (120 μL, 1.62 mmol) in DMF (5 mL). The crude product was purified by silica gel column flash chromatography (30% EE/PE) and recrystallized from ethyl acetate. Yield: 135 mg (76%); $C_{24}H_{16}F_6N_4O_2S_3$ (M_r 602.59); HPLC (purity): 100%; ^{1}H NMR (DMSO-d_6): δ = 12.91 (s, 1 H, N*H*), 8.49 (bs, 1 H, C^7*H*$_{benzth}$), 7.92 (d, ^3J = 8.5 Hz, 1 H, C^4*H*$_{benzth}$), 7.76−7.68 (m, 3 H, C^5*H*$_{benzth}$, C^2*H*$_{benz}$, C^4*H*$_{benz}$), 7.62 (t, ^3J = 7.6 H, 1 H, C^5*H*$_{benz}$), 7.53 (d, ^3J = 7.7 Hz, C^6*H*$_{benz}$), 5.36 (s, 2 H, N-C*H*$_2$), 4.30 (s, 2 H, C*H*$_2$-C=O), 3.28 (t, ^3J = 8.3 Hz, 2 H, SCH$_2$C*H*$_2$), 3.05 (t, ^3J = 8.3 Hz, 2 H, SC*H*$_2$CH$_2$) ppm; ^{13}C NMR (DMSO-d_6): δ = 167.3 (CH$_2$−*C*=O), 161.0 (C$^2_{benzth}$), 160.6 (*C*$_q$N=C-S), 157.8 (N=*C*$_q$-S), 157.1 (NRR'-C=O), 151.3 (C$^{3a}_{benzth}$), 136.4 (*C*$^1_{benz}$), 132.0 (*C*$^{7a}_{benzth}$), 130.9 (*C*^{6}H$_{benz}$), 129.8 (*C*^{5}H$_{benz}$), 129.3 (d, $^2J_{CF}$ = 31.8 Hz, *C*$^3_{benz}$), 124.5 (d, $^1J_{CF}$ = 272.3 Hz, C$^6_{benzth}$-CF$_3$), 124.5 (d, $^3J_{CF}$ = 3.4 Hz, *C*^{2}H$_{benz}$), 124.0 (d, $^1J_{CF}$ = 272.9 Hz, C$^3_{benz}$-CF$_3$), 124.0 (d, $^3J_{CF}$ = 4.2 Hz, *C*^{4}H$_{benz}$), 123.8 (d, $^2J_{CF}$ = 31.2 Hz, C$^6_{benzth}$), 122.9 (d, $^3J_{CF}$ = 4.4 Hz, *C*^{5}H$_{benzth}$), 121.0 (*C*^{4}H$_{benzth}$), 119.9 (d, $^3J_{CF}$ = 4.3 Hz, *C*^{7}H$_{benzth}$), 119.5 (SC$_q$C=O), 46.8 (N-CH$_2$), 36.9 (SCH$_2$CH$_2$), 36.0 (CH$_2$−C=O), 28.4 (SCH$_2$CH$_2$) ppm; MS (ESI, 70 eV) m/z = 602.9 [M + H]$^+$; IR: 3774, 1682, 2987, 1574, 1553, 1331, 1165, 1113, 829, 764, 700 cm^{-1}.

*2-((4-Oxo-3-(4-(trifluoromethyl)benzyl)-3,4,6,7-tetrahydrothieno-[3,2-d]pyrimidin-2-yl)thio)-N-(6-(trifluoromethyl)benzo[d]thiazol-2-yl)acetamide (**22**).* 2-((4-Oxo-3-(4-(trifluoromethyl)benzyl)-3,4,6,7-tetrahydrothieno[3,2-*d*]pyrimidin-2-yl)thio)-*N*-(6-(trifluoromethyl)-benzo[*d*]thiazol-2-yl)acetamide (**22**) was obtained from **16** (104 mg, 0.353 mmol), **14** (114 mg, 0.331 mmol) and triethylamine (140 μL, 1.90 mmol) in DMF (4 mL). The crude product was purified by silica gel column flash chromatography (30% EE/PE). Yield: 155 mg (78%); $C_{24}H_{16}F_6N_4O_2S_3$ (M_r 602.59); HPLC (purity): 99%; ^{1}H NMR (DMSO-d_6): δ = 12.92 (s, 1 H, N*H*), 8.49 (dd, ^4J = 1.2 Hz, ^5J = 0.7 Hz, 1 H, C^7*H*$_{benzth}$), 7.92 (d, ^3J = 8.5 Hz, 1 H, C^4*H*$_{benzth}$), 7.76−7.72 (m, 3 H, C^5*H*$_{benzth}$, C^3*H*$_{benz}$), 7.48 (d, ^3J = 8.0 H, 2 H, C^2*H*$_{benz}$), 5.37 (s, 2 H, N-C*H*$_2$), 4.28 (s, 2 H, C*H*$_2$-C=O), 3.28 (t, ^3J = 8.5 Hz, 2 H, SCH$_2$C*H*$_2$), 3.06 (t, ^3J = 8.3 Hz, 2 H, SC*H*$_2$CH$_2$) ppm; ^{13}C NMR (DMSO-d_6): δ = 167.3 (CH$_2$−*C*=O), 161.0 (C$^2_{benzth}$), 160.6 (*C*$_q$N=C−S), 157.8 (N=*C*$_q$-S), 157.0 (NRR'-C=O), 151.3 (C$^{3a}_{benzth}$), 139.7 (*C*$^1_{benz}$), 131.9 (*C*$^{7a}_{benzth}$), 128.2 (d, $^2J_{CF}$ = 31.9 Hz, *C*$^4_{benz}$), 127.6 (*C*^{2}H$_{benz}$), 125.6 (q, $^3J_{CF}$ = 3.8 Hz, *C*^{3}H$_{benz}$), 124.5 (d, $^1J_{CF}$ = 272.3 Hz, C$^6_{benzth}$-CF$_3$), 124.1 (d, $^1J_{CF}$ = 272.9 Hz, C$^4_{benz}$-CF$_3$), 123.8 (d, $^2J_{CF}$ = 31.9 Hz, C$^6_{benzth}$), 122.9 (d, $^3J_{CF}$ = 3.2 Hz, *C*^{5}H$_{benzth}$), 121.0 (*C*^{4}H$_{benzth}$), 119.9 (d, $^3J_{CF}$ = 3.3 Hz, *C*^{7}H$_{benzth}$), 119.5 (SC$_q$C=O), 46.8 (N-CH$_2$), 36.9 (SCH$_2$CH$_2$), 36.0 (CH$_2$−C=O), 28.4 (SCH$_2$CH$_2$) ppm; MS (ESI, 70 eV) m/z = 602.9 [M + H]$^+$; IR: 3734, 3647, 2910, 1709, 1670, 1553, 1317, 1283, 1109, 1067, 829, 673 cm^{-1}.

DOI: 10.1021/acs.jmedchem.8b00095
J. Med. Chem. 2018, 61, 4087−4102

*2-((4-Oxo-3-(4-(trifluoromethoxy)benzyl)-3,4,6,7-tetrahydrothieno[3,2-d]pyrimidin-2-yl)thio)-N-(6-(trifluoromethyl)-benzo[d]thiazol-2-yl)acetamide (**23**).* 2-((4-Oxo-3-(4-(trifluoromethoxy)benzyl)-3,4,6,7-tetrahydrothieno[3,2-*d*]pyrimidin-2-yl)thio)-*N*-(6-(trifluoromethyl)benzo[*d*]thiazol-2-yl)acetamide (**23**) was obtained from **16** (72.1 mg, 0.245 mmol), **15** (85.0 mg, 0.236 mmol) and triethylamine (100 μL, 1.35 mmol) in DMF (3 mL). The crude product was purified by silica gel column flash chromatography (30% EE/PE). Yield: 105 mg (72%); $C_{24}H_{16}F_6N_4O_3S_3$ (M_r 618.59); HPLC (purity): 98%; ^{1}H NMR (DMSO-d_6): δ = 12.92 (s, 1 H, N*H*), 8.49 (dd, ^4J = 1.2 Hz, ^5J = 0.7 Hz, 1 H, C$^7H_{benzth}$), 7.92 (d, ^3J = 8.5 Hz, 1 H, C$^4H_{benzth}$), 7.74 (dd, ^3J = 8.5 Hz, ^4J = 1.9 Hz, 1 H, C$^5H_{benzth}$), 7.43−7.35 (m, 4 H, C$^2H_{benz}$, C$^3H_{benz}$), 5.29 (s, 2 H, N-CH_2), 4.28 (s, 2 H, CH_2-C═O), 3.27 (t, ^3J = 8.5 Hz, 2 H, SCH$_2$CH_2), 3.04 (t, ^3J = 8.5 Hz, 2 H, SCH_2CH$_2$) ppm; ^{13}C NMR (DMSO-d_6): δ = 167.4 (CH$_2$−C═O), 161.0 (C$^2_{benzth}$), 160.5 (C$_q$N═C−S), 157.8 (N═C$_q$-S), 157.0 (NRR'-C═O), 151.4 (C$^{3a}_{benzth}$), 147.7 (C$^4_{benz}$), 134.4 (C$^1_{benz}$), 132.0 (C$^{7a}_{benzth}$), 129.0 (C^{2}H$_{benz}$), 124.5 ($^1J_{CF}$ = 272.0 Hz, C$^6_{benzth}$-CF$_3$), 123.8 (d, $^2J_{CF}$ = 31.9 Hz, C$^6_{benzth}$), 123.0 (d, $^3J_{CF}$ = 4.4 Hz, C^{5}H$_{benzth}$), 121.3 (C^{3}H$_{benz}$), 121.0 (C^{4}H$_{benzth}$), 120.0 ($^1J_{CF}$ = 256.4 Hz, O-CF$_3$), 119.9 (d, $^3J_{CF}$ = 4.4 Hz, C^{7}H$_{benzth}$), 119.5 (SC$_q$C═O), 46.6 (N-CH$_2$), 36.9 (SCH$_2$CH$_2$), 36.0 (CH$_2$−C═O), 28.4 (SCH$_2$CH$_2$) ppm; MS (ESI, 70 eV) m/z = 619.0 [M + H]$^+$; IR: 2903, 1707, 1672, 1549, 1317, 1265, 1161, 1111, 891, 829, 673 cm^{-1}.

X-ray Analysis of Ligand-Protein Complex (IWP-2 in CK1δ). *Crystallization.* To investigate the binding of **IWP-2** to CK1δ by X-ray crystallography, tCK1δ was expressed and purified as previously described.[53] tCK1δ was co-crystallized with **IWP-2** by using the vapor diffusion sitting drop method. tCK1δ stock solutions (10 mg/mL) were mixed 30:1 with 10 mM **IWP-2** (solubilized in DMSO) and incubated for 30 min at RT. Crystallization trials were set up with drop ratios of 3 μL protein/inhibitor solution to 2 μL precipitant solution. Intergrown crystals appeared after 1 day in drops containing 0.2 M ammonium sulfate, 0.1 M sodium acetate pH 5.25, and 8% (w/v) PEG 2000 MME. A seed stock was prepared from these crystals as described in (Production, Crystallization and Structure Determination of C. difficile PPEP-1 via Microseeding and Zinc-SAD) and used in order to obtain single crystals. Optimization was carried out with drops of 3 μL protein/inhibitor solution and 2 μL precipitant solution. Three μL of water were added, and finally, after 3 h of equilibration, 0.5 μL of 1:3600 seed stock solution was added. Single crystals appeared after 2 days in drops with precipitant solution composing of 0.2 M ammonium sulfate, 0.1 M sodium acetate pH 5.0 and 5% (w/v) PEG 2000 MME. Crystals were flash-cooled in reservoir solution containing 0.3 mM **IWP-2** and 25% (v/v) glycerol.

Data Collection, Phasing, Model Building, and Refinement. Diffraction data were collected at beamline X06DA at the Swiss Light Source, Paul-Scherrer-Institute, Villigen, Switzerland and processed using XDS.[54] The structure was solved by molecular replacement with a truncated crystal structure of CK1δ (PDB ID: 4TWC)[20] as a search model. Between iterative cycles of refinement using phenix.refine[55] missing loops, as well as IWP-2, were manually built with Coot.[56] Restrains of **IWP-2** were calculated using phenix.elbow.[57]

■ ASSOCIATED CONTENT

Supporting Information

The Supporting Information is available free of charge on the ACS Publications website at DOI: 10.1021/acs.jmedchem.8b00095.

Molecular formula strings (CSV)

IC_{50} curves of **IWP** compounds and CK1δ/ε (Supp. Figures 1−2). Selectivity profiling data for **IWP-2** and **19** in a panel of 320 kinases (Supp. Table 1). Kinome Screen and Kinase assay results for TLK2 and ZAP70 (Supp. Figure 3). X-ray analysis of **IWP-2** in CK1δ (pdb 5OKT) (Supp. Table 2, Supp. Figure 4). EC_{50} curves of **IWP** compounds on various cancer cell lines (Supp. Figures 5−7). Synthesis of isothiocyanate precursors (Supp. Figure 8). IC_{50} curves of IWP derivatives (Supp. Figures 9−11). Screening of IWP derivatives on CK1α and CK1γ3 (Supp. Figure 12). Effect of compounds on Wnt signaling (Supp. Figure 13) (PDF)

Accession Codes

Authors will release the atomic coordinates and experimental data upon article publication. Co-crystallization of **IWP-2** in CK1δ: 5OKT.

■ AUTHOR INFORMATION

Corresponding Authors

*Tel. 0049 731 500 53580. Fax 0049 731 500 53582. E-mail: uwe.knippschild@uniklinik-ulm.de.

*Tel. 0049 431 880 1137. Fax 0049 431 880 1352. E-mail: cpeifer@pharmazie.uni-kiel.de.

ORCID

Christian Peifer: 0000-0003-1532-7826

Author Contributions

B.G.-R. and L.W. contributed equally, and C.P. and U.K. are considered senior authors.

Notes

The authors declare no competing financial interest.

■ ACKNOWLEDGMENTS

B.G.-R was kindly supported by the German Academic Exchange Service (DAAD). D.S. acknowledges financial support by the German Federal Ministry of Education and Research (BMBF, Grant 131605). We gratefully recognize the help of Martin Schütt und Dr. Ulrich Girreser, University of Kiel, Institute of Pharmacy, Germany, for analytical assistance. Work in the lab of Uwe Knippschild was supported by the DFG (KN356/6-1, and SFB 1149, project B04 to UK and MW). The crystallographic experiments leading to these results have received funding from the European Community's Seventh Framework Programme (FP7/2007-2013) under grant agreement no. 283570 (BioStruct-X).

■ ABBREVIATIONS USED

ATP, adenosine triphosphate; CK1, protein kinase; CK1, formerly known as casein kinase 1; HPI, hydrophobic pocket I; HRII, hydrophobic region II; IWP, inhibitors of Wnt production; PDB, Research Collaboratory for Structural Bioinformatics (RCSB) Protein Data Bank; Porcn, Porcupine; MBOAT, member of membrane-bound O-acyltransferases

■ REFERENCES

(1) Knippschild, U.; Kruger, M.; Richter, J.; Xu, P.; Garcia-Reyes, B.; Peifer, C.; Halekotte, J.; Bakulev, V.; Bischof, J. The CK1 family: contribution to cellular stress response and its role in carcinogenesis. *Front. Oncol.* **2014**, *4* (96), 1−32.

(2) Price, M. H.; Roberts, D. M.; McCartney, B. M.; Jezuit, E.; Peifer, M. Cytoskeletal dynamics and cell signaling during planar polarity establishment in the Drosophila embryonic denticle. *J. Cell Sci.* **2006**, *119* (3), 403−415.

(3) Cheong, J. K.; Virshup, D. M. Casein kinase 1: complexity in the family. *Int. J. Biochem. Cell Biol.* **2011**, *43* (4), 465−469.

(4) (a) Green, C. L.; Bennett, G. S. Identification of four alternatively spliced isoforms of chicken casein kinase I alpha that are all expressed in diverse cell types. *Gene* **1998**, *216* (1), 189−195. (b) Fu, Z.; Chakraborti, T.; Morse, S.; Bennett, G. S.; Shaw, G. Four casein kinase I isoforms are differentially partitioned between nucleus and cytoplasm. *Exp. Cell Res.* **2001**, *269* (2), 275−286. (c) Burzio, V.; Antonelli, M.; Allende, C. C.; Allende, J. E. Biochemical and cellular

DOI: 10.1021/acs.jmedchem.8b00095
J. Med. Chem. 2018, 61, 4087−4102

characteristics of the four splice variants of protein kinase CK1alpha from zebrafish (Danio rerio). *J. Cell. Biochem.* **2002**, *86* (4), 805−814.
(5) (a) Graves, P. R.; Haas, D. W.; Hagedorn, C. H.; DePaoli-Roach, A. A.; Roach, P. J. Molecular cloning, expression, and characterization of a 49-kilodalton casein kinase I isoform from rat testis. *J. Biol. Chem.* **1993**, *268* (9), 6394−6401. (b) Fish, K. J.; Cegielska, A.; Getman, M. E.; Landes, G. M.; Virshup, D. M. Isolation and characterization of human casein kinase I ε (CKI), a novel member of the CKI gene family. *J. Biol. Chem.* **1995**, *270* (25), 14875−14883. (c) Zhai, L.; Graves, P. R.; Robinson, L. C.; Italiano, M.; Culbertson, M. R.; Rowles, J.; Cobb, M. H.; DePaoli-Roach, A. A.; Roach, P. J. Casein kinase I gamma subfamily. Molecular cloning, expression, and characterization of three mammalian isoforms and complementation of defects in the Saccharomyces cerevisiae YCK genes. *J. Biol. Chem.* **1995**, *270* (21), 12717−12724.
(6) Gross, S. D.; Anderson, R. A. Casein kinase I: spatial organization and positioning of a multifunctional protein kinase family. *Cell. Signalling* **1998**, *10* (10), 699−711.
(7) Niehrs, C. The complex world of WNT receptor signalling. *Nat. Rev. Mol. Cell Biol.* **2012**, *13* (12), 767−779.
(8) Nusse, R. Wnt signaling. *Cold Spring Harbor Perspect. Biol.* **2012**, *4* (5), a011163.
(9) Cruciat, C. M. Casein kinase 1 and Wnt/beta-catenin signaling. *Curr. Opin. Cell Biol.* **2014**, *31*, 46−55.
(10) (a) Cheong, J. K.; Hung, T. H.; Wang, H.; Tan, P.; Voorhoeve, P. M.; Lee, S. H.; Virshup, D. M. IC261 induces cell cycle arrest and apoptosis of human cancer cells via CK1δ/ε and Wnt/β-catenin independent inhibition of mitotic spindle formation. *Oncogene* **2011**, *30* (22), 2558−2569. (b) Umar, S.; Wang, Y.; Morris, A. P.; Sellin, J. H. Dual alterations in casein kinase I-ε and GSK-3beta modulate beta-catenin stability in hyperproliferating colonic epithelia. *Am. J. Physiol. Gastrointest. Liver* **2007**, *292* (2), 599−607.
(11) Davidson, G.; Wu, W.; Shen, J.; Bilic, J.; Fenger, U.; Stannek, P.; Glinka, A.; Niehrs, C. Casein kinase 1 gamma couples Wnt receptor activation to cytoplasmic signal transduction. *Nature* **2005**, *438* (7069), 867−872.
(12) Swiatek, W.; Kang, H.; Garcia, B. A.; Shabanowitz, J.; Coombs, G. S.; Hunt, D. F.; Virshup, D. M. Negative regulation of LRP6 function by casein kinase I ε phosphorylation. *J. Biol. Chem.* **2006**, *281* (18), 12233−12241.
(13) Peters, J. M.; McKay, R. M.; McKay, J. P.; Graff, J. M. Casein kinase I transduces Wnt signals. *Nature* **1999**, *401* (6751), 345−350.
(14) Cruciat, C. M.; Niehrs, C. Secreted and transmembrane wnt inhibitors and activators. *Cold Spring Harbor Perspect. Biol.* **2013**, *5* (3), a015081.
(15) Kahn, M. Can we safely target the WNT pathway? *Nat. Rev. Drug Discovery* **2014**, *13* (7), 513−532.
(16) Wang, X.; Moon, J.; Dodge, M. E.; Pan, X.; Zhang, L.; Hanson, J. M.; Tuladhar, R.; Ma, Z.; Shi, H.; Williams, N. S.; Amatruda, J. F.; Carroll, T. J.; Lum, L.; Chen, C. The development of highly potent inhibitors for porcupine. *J. Med. Chem.* **2013**, *56* (6), 2700−2704.
(17) Chen, B.; Dodge, M. E.; Tang, W.; Lu, J.; Ma, Z.; Fan, C. W.; Wei, S.; Hao, W.; Kilgore, J.; Williams, N. S.; Roth, M. G.; Amatruda, J. F.; Chen, C.; Lum, L. Small molecule-mediated disruption of Wnt-dependent signaling in tissue regeneration and cancer. *Nat. Chem. Biol.* **2009**, *5* (2), 100−107.
(18) Wang, S.; Yin, J.; Chen, D.; Nie, F.; Song, X.; Fei, C.; Miao, H.; Jing, C.; Ma, W.; Wang, L.; Xie, S.; Li, C.; Zeng, R.; Pan, W.; Hao, X.; Li, L. Small-molecule modulation of Wnt signaling via modulating the Axin-LRP5/6 interaction. *Nat. Chem. Biol.* **2013**, *9* (9), 579−585.
(19) Takada, R.; Satomi, Y.; Kurata, T.; Ueno, N.; Norioka, S.; Kondoh, H.; Takao, T.; Takada, S. Monounsaturated fatty acid modification of Wnt protein: its role in Wnt secretion. *Dev. Cell* **2006**, *11* (6), 791−801.
(20) Bischof, J.; Leban, J.; Zaja, M.; Grothey, A.; Radunsky, B.; Othersen, O.; Strobl, S.; Vitt, D.; Knippschild, U. 2-Benzamido-N-(1H-benzo[d]imidazol-2-yl)thiazole-4-carboxamide derivatives as potent inhibitors of CK1δ/ε. *Amino Acids* **2012**, *43* (4), 1577−1591.
(21) Schade, D.; Plowright, A. T. Medicinal chemistry approaches to heart regeneration. *J. Med. Chem.* **2015**, *58* (24), 9451−9479.
(22) Rao, J.; Pfeiffer, M. J.; Frank, S.; Adachi, K.; Piccini, I.; Quaranta, R.; Arauzo-Bravo, M.; Schwarz, J.; Schade, D.; Leidel, S.; Scholer, H. R.; Seebohm, G.; Greber, B. Stepwise clearance of repressive roadblocks drives cardiac induction in human ESCs. *Cell Stem Cell* **2016**, *18* (4), 554−560.
(23) Salado, I. G.; Redondo, M.; Bello, M. L.; Perez, C.; Liachko, N. F.; Kraemer, B. C.; Miguel, L.; Lecourtois, M.; Gil, C.; Martinez, A.; Perez, D. I. Protein kinase CK-1 inhibitors as new potential drugs for amyotrophic lateral sclerosis. *J. Med. Chem.* **2014**, *57* (6), 2755−2772.
(24) Richter, J.; Bischof, J.; Zaja, M.; Kohlhof, H.; Othersen, O.; Vitt, D.; Alscher, V.; Pospiech, I.; Garcia-Reyes, B.; Berg, S.; Leban, J.; Knippschild, U. Difluoro-dioxolo-benzoimidazol-benzamides as potent inhibitors of CK1δ and ε with nanomolar inhibitory activity on cancer cell proliferation. *J. Med. Chem.* **2014**, *57* (19), 7933−7946.
(25) Peifer, C.; Abadleh, M.; Bischof, J.; Hauser, D.; Schattel, V.; Hirner, H.; Knippschild, U.; Laufer, S. 3,4-Diaryl-isoxazoles and -imidazoles as potent dual inhibitors of p38alpha mitogen activated protein kinase and casein kinase 1δ. *J. Med. Chem.* **2009**, *52* (23), 7618−7630.
(26) Anderson, K. M.; Alrefai, W. A.; Bonomi, P.; Dudeja, P.; Ou, D.; Anderson, C.; Harris, J. E. Altered oncogene, tumor suppressor and cell-cycle gene expression in PANC-1 cells cultured with the pleiotrophic 5-lipoxygenase inhibitor, MK886, assessed with a gene chip. *Anticancer Res.* **1999**, *19* (5B), 3873−3887.
(27) (a) Brockschmidt, C.; Hirner, H.; Huber, N.; Eismann, T.; Hillenbrand, A.; Giamas, G.; Radunsky, B.; Ammerpohl, O.; Bohm, B.; Henne-Bruns, D.; Kalthoff, H.; Leithauser, F.; Trauzold, A.; Knippschild, U. Anti-apoptotic and growth-stimulatory functions of CK1 δ and ε in ductal adenocarcinoma of the pancreas are inhibited by IC261 in vitro and in vivo. *Gut* **2008**, *57* (6), 799−806. (b) Long, A.; Zhao, H.; Huang, X. Structural basis for the interaction between casein kinase 1 δ and a potent and selective inhibitor. *J. Med. Chem.* **2012**, *55*, 956−960.
(28) Bauwens, C. L.; Toms, D.; Ungrin, M. Aggregate size optimization in microwells for suspension-based cardiac differentiation of human pluripotent stem cells. *J. Visualized Exp.* **2016**, *115*, 1−8.
(29) Piccini, I.; Arauzo-Bravo, M.; Seebohm, G.; Greber, B. Functional high-resolution time-course expression analysis of human embryonic stem cells undergoing cardiac induction. *Genomics Data* **2016**, *10*, 71−74.
(30) Zanella, F.; Sheikh, F. Patient-specific induced pluripotent stem cell models: generation and characterization of cardiac cells. *Methods Mol. Biol.* **2014**, *1353*, 147−162.
(31) ten Berge, D.; Kurek, D.; Blauwkamp, T.; Koole, W.; Maas, A.; Eroglu, E.; Siu, R. K.; Nusse, R. Embryonic stem cells require Wnt proteins to prevent differentiation to epiblast stem cells. *Nat. Cell Biol.* **2011**, *13* (9), 1070−1075.
(32) Hernandez-Nunez, E.; Tlahuext, H.; Moo-Puc, R.; Torres-Gomez, H.; Reyes-Martinez, R.; Cedillo-Rivera, R.; Nava-Zuazo, C.; Navarrete-Vazquez, G. Synthesis and in vitro trichomonicidal, giardicidal and amebicidal activity of N-acetamide(sulfonamide)-2-methyl-4-nitro-1H-imidazoles. *Eur. J. Med. Chem.* **2009**, *44* (7), 2975−2984.
(33) Lanier, M.; Schade, D.; Willems, E.; Tsuda, M.; Spiering, S.; Kalisiak, J.; Mercola, M.; Cashman, J. R. Wnt inhibition correlates with human embryonic stem cell cardiomyogenesis: a structure-activity relationship study based on inhibitors for the Wnt response. *J. Med. Chem.* **2012**, *55* (2), 697−708.
(34) Dietrich, L.; Rathmer, B.; Ewan, K.; Bange, T.; Heinrichs, S.; Dale, T. C.; Schade, D.; Grossmann, T. N. Cell permeable stapled peptide inhibitor of Wnt signaling that targets beta-catenin protein-protein interactions. *Cell Chem. Biol.* **2017**, *24* (8), 958−968.
(35) Cheng, Y.; Phoon, Y. P.; Jin, X.; Chong, S. Y.; Ip, J. C.; Wong, B. W.; Lung, M. L. Wnt-C59 arrests stemness and suppresses growth of nasopharyngeal carcinoma in mice by inhibiting the Wnt pathway in the tumor microenvironment. *Oncotarget* **2015**, *6* (16), 14428−14439.

DOI: 10.1021/acs.jmedchem.8b00095
J. Med. Chem. 2018, 61, 4087−4102

(36) Proffitt, K. D.; Madan, B.; Ke, Z.; Pendharkar, V.; Ding, L.; Lee, M. A.; Hannoush, R. N.; Virshup, D. M. Pharmacological inhibition of the Wnt acyltransferase PORCN prevents growth of WNT-driven mammary cancer. *Cancer Res.* **2013**, *73* (2), 502−507.
(37) Auld, D. S.; Southall, N. T.; Jadhav, A.; Johnson, R. L.; Diller, D. J.; Simeonov, A.; Austin, C. P.; Inglese, J. Characterization of chemical libraries for luciferase inhibitory activity. *J. Med. Chem.* **2008**, *51* (8), 2372−2386.
(38) Hammerlein, A.; Weiske, J.; Huber, O. A second protein kinase CK1-mediated step negatively regulates Wnt signalling by disrupting the lymphocyte enhancer factor-1/beta-catenin complex. *Cell. Mol. Life Sci.* **2005**, *62* (5), 606−618.
(39) Duong-Ly, K. C.; Devarajan, K.; Liang, S.; Horiuchi, K. Y.; Wang, Y.; Ma, H.; Peterson, J. R. Kinase inhibitor profiling reveals unexpected opportunities to inhibit disease-associated mutant kinases. *Cell Rep.* **2016**, *14* (4), 772−781.
(40) Sillibourne, J. E.; Milne, D. M.; Takahashi, M.; Ono, Y.; Meek, D. W. Centrosomal anchoring of the protein kinase CK1δ mediated by attachment to the large, coiled-coil scaffolding protein CG-NAP/AKAP450. *J. Mol. Biol.* **2002**, *322* (4), 785−797.
(41) Knippschild, U.; Milne, D. M.; Campbell, L. E.; DeMaggio, A. J.; Christenson, E.; Hoekstra, M. F.; Meek, D. W. p53 is phosphorylated in vitro and in vivo by the δ and ε isoforms of casein kinase 1 and enhances the level of casein kinase 1 δ in response to topoisomerase-directed drugs. *Oncogene* **1997**, *15* (14), 1727−1736.
(42) Wolff, S.; Xiao, Z.; Wittau, M.; Sussner, N.; Stoter, M.; Knippschild, U. Interaction of casein kinase 1 δ (CK1 δ) with the light chain LC2 of microtubule associated protein 1A (MAP1A). *Biochim. Biophys. Acta, Mol. Cell Res.* **2005**, *1745* (2), 196−206.
(43) Knippschild, U.; Milne, D.; Campbell, L.; Meek, D. p53 N-terminus-targeted protein kinase activity is stimulated in response to wild type p53 and DNA damage. *Oncogene* **1996**, *13* (7), 1387−1393.
(44) Meng, Z.; Bischof, J.; Ianes, C.; Henne-Bruns, D.; Xu, P.; Knippschild, U. CK1δ kinase activity is modulated by protein kinase C alpha (PKCalpha)-mediated site-specific phosphorylation. *Amino Acids* **2016**, *48* (5), 1185−1197.
(45) Yunis, A. A.; Arimura, G. K.; Russin, D. J. Human pancreatic carcinoma (MIA PaCa-2) in continuous culture: sensitivity to asparaginase. *Int. J. Cancer* **1977**, *19* (1), 128−135.
(46) Lieber, M.; Mazzetta, J.; Nelson-Rees, W.; Kaplan, M.; Todaro, G. Establishment of a continuous tumor-cell line (panc-1) from a human carcinoma of the exocrine pancreas. *Int. J. Cancer* **1975**, *15* (5), 741−747.
(47) Thomas, P.; Smart, T. G. HEK293 cell line: a vehicle for the expression of recombinant proteins. *J. Pharmacol. Toxicol. Methods* **2005**, *51* (3), 187−200.
(48) Polak-Charcon, S.; Ben-Shaul, Y. Degradation of tight junctions in HT29, a human colon adenocarcinoma cell line. *J. Cell Sci.* **1979**, *35*, 393−402.
(49) Okabe, T.; Sasaki, N.; Matsuzaki, M.; Imai, Y.; Kaneko, Y.; Matsuzaki, F.; Takaku, F.; Tsushima, T. Establishment and characterization of a new human functional cell line from a choriocarcinoma. *Cancer Res.* **1983**, *43* (10), 4920−4926.
(50) Lehnert, L.; Lerch, M. M.; Hirai, Y.; Kruse, M. L.; Schmiegel, W.; Kalthoff, H. Autocrine stimulation of human pancreatic duct-like development by soluble isoforms of epimorphin in vitro. *J. Cell Biol.* **2001**, *152* (5), 911−922.
(51) Leibovitz, A.; Stinson, J. C.; McCombs, W. B., 3rd; McCoy, C. E.; Mazur, K. C.; Mabry, N. D. Classification of human colorectal adenocarcinoma cell lines. *Cancer Res.* **1976**, *36* (12), 4562−4569.
(52) Willert, K.; Brown, J. D.; Danenberg, E.; Duncan, A. W.; Weissman, I. L.; Reya, T.; Yates, J. R., 3rd; Nusse, R. Wnt proteins are lipid-modified and can act as stem cell growth factors. *Nature* **2003**, *423* (6938), 448−452.
(53) Halekotte, J.; Witt, L.; Ianes, C.; Kruger, M.; Buhrmann, M.; Rauh, D.; Pichlo, C.; Brunstein, E.; Luxenburger, A.; Baumann, U.; Knippschild, U.; Bischof, J.; Peifer, C. Optimized 4,5-diarylimidazoles as potent/selective inhibitors of protein kinase CK1δ and their structural relation to p38alpha MAPK. *Molecules* **2017**, *22* (4), 522.
(54) Kabsch, W. Xds. *Acta Crystallogr., Sect. D: Biol. Crystallogr.* **2010**, *66* (2), 125−132.
(55) Afonine, P. V.; Grosse-Kunstleve, R. W.; Echols, N.; Headd, J. J.; Moriarty, N. W.; Mustyakimov, M.; Terwilliger, T. C.; Urzhumtsev, A.; Zwart, P. H.; Adams, P. D. Towards automated crystallographic structure refinement with phenix.refine. *Acta Crystallogr., Sect. D: Biol. Crystallogr.* **2012**, *68* (4), 352−367.
(56) Emsley, P.; Lohkamp, B.; Scott, W. G.; Cowtan, K. Features and development of Coot. *Acta Crystallogr., Sect. D: Biol. Crystallogr.* **2010**, *66* (4), 486−501.
(57) Moriarty, N. W.; Grosse-Kunstleve, R. W.; Adams, P. D. Electronic Ligand Builder and Optimization Workbench (eLBOW): a tool for ligand coordinate and restraint generation. *Acta Crystallogr., Sect. D: Biol. Crystallogr.* **2009**, *65* (10), 1074−1080.

DOI: 10.1021/acs.jmedchem.8b00095
J. Med. Chem. 2018, 61, 4087−4102